Applied Numerical Mathematics 137 (2019) 230–251

Contents lists available at ScienceDirect

Applied Numerical Mathematics

www.elsevier.com/locate/apnum

The design of conservative finite element discretisations for the vectorial modified KdV equation ☆

James Jackaman [a,*], Georgios Papamikos [b], Tristan Pryer [a]

[a] Department of Mathematics and Statistics, University of Reading, Reading RG6 6AX, UK
[b] School of Mathematics, University of Leeds, Leeds LS2 9JT, UK

ARTICLE INFO

Article history:
Received 12 February 2018
Received in revised form 16 October 2018
Accepted 20 October 2018
Available online 30 October 2018

Keywords:
Hamiltonian PDE
Conservative finite element method
Vectorial modified KdV equation

ABSTRACT

We design a consistent Galerkin scheme for the approximation of the vectorial modified Korteweg–de Vries equation with periodic boundary conditions. We demonstrate that the scheme conserves energy up to solver tolerance. In this sense the method is consistent with the energy balance of the continuous system. This energy balance ensures there is no numerical dissipation allowing for extremely accurate long time simulations free from numerical artifacts. Various numerical experiments are shown demonstrating the asymptotic convergence of the method with respect to the discretisation parameters. Some simulations are also presented that correctly capture the unusual interactions between solitons in the vectorial setting.

1. Introduction

Hamiltonian partial differential equations (PDEs) are a specific class of PDE endowed with physically relevant algebraic and geometric structures [33]. They arise from a variety of areas [40], not least meteorological, such as the semi-geostrophic equations [37], and oceanographical, such as the Korteweg–de Vries (KdV) and nonlinear Schrödinger equations [31]. The KdV and nonlinear Schrödinger equations are particularly special examples, in that they are bi-Hamiltonian [29]. This means they have two different Hamiltonian formulations which, in turn, is one way to understand the notion of *integrability* of these problems. Regardless, the applications and the need to quantify the dynamics of the general Cauchy problem motivate the development of accurate long time simulations for reliable prediction of dynamics in both meteorology and oceanography.

A difficulty in the design of schemes for this class of problems is that the long term dynamics of solutions can be destroyed by the addition of *artificial numerical diffusion*. The reason for inclusion of this in a given scheme is the desirable stability properties this endows on the approximation, however, this typically destroys all information in the long term dynamics of the system through smearing of solutions.

Conservative schemes for Hamiltonian ordinary differential equations (ODEs) are relatively well understood, see [13,28, 20,8,7, cf.]. Typically numerical schemes designed for this class of problem which have some property of the ODE built into them, for example conservativity of the Hamiltonian or the underlying symplectic form, are classified as geometric

☆ JJ was supported through a PhD scholarship awarded by the "EPSRC Centre for Doctoral Training in the Mathematics of Planet Earth at Imperial College London and the University of Reading" EP/L016613/1. TP was partially supported through the EPSRC grant EP/P000835/1. GP was partially supported through a Rado Postdoctoral fellowship at the University of Reading and the EPSRC grant EP/P012655/1. All this support is gratefully acknowledged.

* Corresponding author.
E-mail addresses: James.Jackaman@pgr.reading.ac.uk (J. Jackaman), G.Papamikos@leeds.ac.uk (G. Papamikos), T.Pryer@reading.ac.uk (T. Pryer).

https://doi.org/10.1016/j.apnum.2018.10.006
0168-9274/

integrators. In the PDE setting symplectic structure preserving algorithms have also been developed [35,12,14,15]. Here the PDEs are rewritten using their corresponding symplectic form, and the notion of structure preservation is given in terms of a discrete (difference) conservation law involving differential forms. Typically these problems are solved using an Euler/Preissman box scheme, although space–time finite element methods under an appropriate quadrature choice form a natural generalisation. Another promising mechanism to approximate such problems is based on the Fokas transform [26] which experimentally has extremely good long time properties as the scheme naturally inherits many of the properties of the PDE.

In this contribution we consider a system of equations that are a multidimensional generalisation of the famous modified KdV equation

$$u_t + \frac{3}{2}u^2 u_x + u_{xxx} = 0,$$

where the subindices denote partial differentiation with respect to the corresponding independent variable. This equation has numerous applications not least including fluid dynamics and plasma physics [1]. The vectorial equation [30] appears frequently in the study of ocean waves and Riemannian geometry [39,3,2]. The presence of the Korteweg third order term as well as the lack of sign in the corresponding energy functional, further details given in §2, can cause issues in the numerical treatment of this problem. The vectorial equation also has additional complications that do not arise in the scalar setting. Indeed, the underlying conservation laws themselves have a vastly different structure, for example there is no mass conservation in the vectorial case. Moreover, the corresponding Hamiltonian operator is a nonlocal differential operator in the vectorial case.

In previous numerical studies of the scalar KdV and modified KdV equations [42,43, cf.], it has been observed that classical finite volume and discontinuous Galerkin (dG) schemes with "standard" numerical fluxes introduce numerical artifacts. These typically appear through numerical regularisation effects included for stability purposes that are not, however, adapted to the variational structure of the problem. The result of these artifacts is an inconsistency in the discrete energy.

Hamiltonian problems are inherently conservative, that is, the underlying Hamiltonian is conserved over time. Other equations, including those of integrable type, may have additional structures that manifest themselves through additional conserved quantities. In particular, mass and momentum are such quantities. In [11] and [25] the authors propose and analyse a dG scheme for generalised KdV equations. The scheme itself is very carefully designed to be conservative, in that the invariant corresponding to the *momentum* is inherited by the discretisation. This yields L^2 stability quite naturally in the numerical scheme and extremely good long time dynamics. In the scalar case one may also design schemes that conserve the energy itself [41,24], however, it does not seem possible to design schemes to conserve more than two of these invariants.

When examining the case of systems of Hamiltonian equations much less work has been carried out, for example [4] give a near conservative method for a system of Schrödinger–KdV type and [10] study a system of KdV equations. To the authors knowledge there has not been any work on the system we study, nor such Hamiltonian systems in general. Our goal in this work is the derivation of Galerkin discretisations aimed at preserving the underlying algebraic properties satisfied by the PDE system whilst avoiding the introduction of stabilising diffusion terms. Our schemes are therefore consistent with (one of) the Hamiltonian formulation of the original problem. It is important to note that our approach is not an adaptation of entropy conserving schemes developed for systems of conservation laws, rather we study the algebraic properties of the PDE and formulate the discretisation to inherit this specific structure. The methods are of arbitrarily high order of accuracy in space and provide relevant approximations free from numerical artifacts. To the authors knowledge this is the first class of finite element method for this particular class of system to have these properties although similar techniques have proven useful in the study of dispersive phase flow problems [17,18].

The rest of this work is set out as follows: In §2 we introduce notation, the model problem and some of its properties. We give a reformulation of the system through the introduction of auxiliary variables, these are introduced to allow for a simple construction of the numerical scheme. In §3 we examine a temporal discretisation of the problem that guarantees the conservation of the underlying Hamiltonian. In §4 we propose a spatial discretisation based on continuous finite elements, state a fully discrete method and show that it is conservative. Finally in §5 we summarise extensive numerical experiments aimed at testing the robustness of the method particularly in long time simulations.

2. The vectorial modified KdV equation

In this section we formulate the model problem, fix notation and give some basic assumptions. We describe some known results and history of the vectorial modified Korteweg–de Vries (vmKdV) equation, highlighting the Hamiltonian structure of the equation. We show that the underlying Hamiltonian structure naturally yields an induced stability of the solutions to the PDE system and give a brief description of how to construct some exact solutions using a dressing method. We then show how the system can be written through induced auxiliary variables which are the basis of the design of our numerical scheme.

Throughout this work we denote the standard Lebesgue spaces by $L^p(\omega)$ for $\omega \subseteq \mathbb{R}$, $p \in [1, \infty]$, equipped with corresponding norms $\|u\|_{L^p(\omega)}$. In addition, we will denote $H^k(\omega)$ to be the Hilbert space of order k of real-valued functions defined over $\omega \subseteq \mathbb{R}$ with norm $\|u\|_{H^k(\omega)}$.

The vmKdV equation is an evolutionary PDE for a real, d-vector valued function

$$\begin{array}{rccl} \boldsymbol{u}: & \mathbb{R}^2 & \to & \mathbb{R}^d \\ & (x,t) & \mapsto & \boldsymbol{u}(x,t) = (u_1 \ldots, u_d)^\intercal \end{array} \tag{2.1}$$

and is given by

$$\boldsymbol{u}_t + \frac{3}{2}\boldsymbol{u}\cdot\boldsymbol{u}\boldsymbol{u}_x + \boldsymbol{u}_{xxx} = \boldsymbol{0}. \tag{2.2}$$

Here we are using "$\boldsymbol{x}\cdot\boldsymbol{y}$" as the Euclidean inner product between two vectors, $\boldsymbol{x}$ and $\boldsymbol{y}$ and "$|\boldsymbol{x}|$" as the induced Euclidean norm of $\boldsymbol{x}$.

A particular case of the vmKdV system occurs when $d=2$, $\boldsymbol{u}=(u_1,u_2)^\intercal$ when (2.2) can be identified with the complex modified KdV (mKdV) equation

$$y_t + \frac{3}{2}|y|^2 y_x + y_{xxx} = 0 \tag{2.3}$$

for the complex dependent variable $y = u_1 + iu_2$. Sometimes this is also called the Hirota mKdV equation [21]. When $d=1$ we obtain the famous mKdV equation which has been studied numerically in the context of Galerkin methods in [11,24].

Equation (2.2) admits both Lie and discrete point symmetries and has infinitely many conservation laws. Indeed, under the action of the orthogonal group $O_d(\mathbb{R})$, which is the group of real $d\times d$ matrices such that $\boldsymbol{A}^\intercal\boldsymbol{A}=\mathbf{I}$,

$$\widetilde{\boldsymbol{u}} = \boldsymbol{A}\boldsymbol{u}, \quad \text{for } \boldsymbol{A}\in O_d(\mathbb{R}) \tag{2.4}$$

equation (2.2) remains invariant. Moreover, vmKdV is invariant under the translations

$$\widetilde{x} = x+\epsilon, \quad \widetilde{t} = t+\gamma \tag{2.5}$$

and under the scaling transformation

$$\left(\widetilde{x},\widetilde{t},\widetilde{\boldsymbol{u}}\right) = \left(e^{\epsilon}x, e^{3\epsilon}t, e^{-\epsilon}\boldsymbol{u}\right). \tag{2.6}$$

2.1 Proposition *(Conservative properties of solutions). The vmKdV equation admits the following conservation laws:*

$$\begin{aligned} &\mathrm{D}_t f_2(\boldsymbol{u}) = \mathrm{D}_x g_2(\boldsymbol{u}) \\ &\mathrm{D}_t f_4(\boldsymbol{u}) = \mathrm{D}_x g_4(\boldsymbol{u}), \end{aligned} \tag{2.7}$$

where the conserved densities are given by

$$\begin{aligned} f_2(\boldsymbol{u}) &= \frac{1}{2}|\boldsymbol{u}|^2 \\ f_4(\boldsymbol{u}) &= \frac{1}{2}|\boldsymbol{u}_x|^2 - \frac{1}{8}|\boldsymbol{u}|^4 \end{aligned} \tag{2.8}$$

and the corresponding fluxes are

$$\begin{aligned} g_2(\boldsymbol{u}) &= |\boldsymbol{u}_x|^2 - 2\boldsymbol{u}\cdot\boldsymbol{u}_{xx} - \frac{3}{4}|\boldsymbol{u}|^4 \\ g_4(\boldsymbol{u}) &= \frac{1}{8}|\boldsymbol{u}|^6 - |\boldsymbol{u}|^2|\boldsymbol{u}_x|^2 - \frac{1}{2}(\boldsymbol{u}\cdot\boldsymbol{u}_x)^2 - \boldsymbol{u}_x\cdot\boldsymbol{u}_{xxx} + \frac{1}{2}|\boldsymbol{u}_{xx}|^2 + \frac{1}{2}|\boldsymbol{u}|^2\boldsymbol{u}\cdot\boldsymbol{u}_{xx}. \end{aligned} \tag{2.9}$$

Proof. To prove that the total time derivative of $f_2(\mathbf{u})$ and $f_4(\mathbf{u})$ are in the image of D_x we use the Euler operator $\boldsymbol{E} = (E_1, \ldots, E_d)$, where

$$E_i(f) = \sum_{k=0}^{\infty}(-D_x)^k \partial_{u_{i_{kx}}} f, \quad u_{i_{kx}} = u_{i\underbrace{x\ldots x}_{k}}$$

and the fact that $\mathrm{Ker}\boldsymbol{E} = \mathrm{Im}D_x$, see [33] for a proof. On the other hand in order to calculate the corresponding fluxes g_2 and g_4 we apply the homotopy operator [33] to $D_t f_2(\mathbf{u})$ and $D_t f_4(\mathbf{u})$ respectively. The homotopy operator is given by

$$H(f(\mathbf{u})) = \int_0^1 \sum_{i=1}^{d} \mathrm{I}_i(f)(\lambda\mathbf{u})\frac{d\lambda}{\lambda}$$

where

$$\mathrm{I}_i(f) = \sum_{k=1}^{\infty} \left(\sum_{s=0}^{k-1} u_{i_{sx}} (-D_x)^{k-s-1} \right) f_{u_{i_{kx}}}. \quad \square$$

2.2 Corollary. *Let $\mathbb{S}^1$ be the unitary circle, i.e., $[0,1]$ with matching endpoints. Then from Proposition 2.1 it follows that, upon defining*

$$F_2(\boldsymbol{u}) := \int_{\mathbb{S}^1} f_2(\boldsymbol{u})\,\mathrm{d}x \tag{2.10}$$

as the momentum *functional and*

$$F_4(\boldsymbol{u}) := \int_{\mathbb{S}^1} f_4(\boldsymbol{u})\,\mathrm{d}x \tag{2.11}$$

as the energy *functional for periodic solutions we have*

$$\mathrm{D}_t F_2(\boldsymbol{u}) = \mathrm{D}_t F_4(\boldsymbol{u}) = 0. \tag{2.12}$$

Moreover this does not just hold for periodic solutions over $\mathbb{S}^1$. Indeed, one can consider the equation (2.2) over $\mathbb{R}$ and require that solutions decay at infinity, for example Schwartz functions, and the result holds. A particular example of such solutions are the much celebrated soliton and breather solutions. The conservation laws also allow for the a priori control of the solution.

2.3 Proposition *(Stability bound). Let the vmKdV system (2.2), defined over $\mathbb{S}^1$, be coupled with initial conditions $\boldsymbol{u}_0$ satisfying $F_2(\boldsymbol{u}_0) = C_2 < \infty$ and $F_4(\boldsymbol{u}_0) = C_4 < \infty$ then $\boldsymbol{u}$ satisfies*

$$\|\boldsymbol{u}_x(t)\|_{\mathrm{L}^2(\mathbb{S}^1)} \leq \left(4C_4 + \frac{C_{GN}^8 C_2^3}{2} \right)^{1/2}, \tag{2.13}$$

where C_{GN} is a constant appearing from the Gagliardo–Nirenberg interpolation inequality.

Proof. In view of the definition of $F_4(\boldsymbol{u})$ we have that

$$\begin{aligned} \|\boldsymbol{u}_x\|^2_{\mathrm{L}^2(\mathbb{S}^1)} &= 2F_4(\boldsymbol{u}) + \frac{1}{4}\|\boldsymbol{u}\|^4_{\mathrm{L}^4(\mathbb{S}^1)} \\ &= 2F_4(\boldsymbol{u}_0) + \frac{1}{4}\|\boldsymbol{u}\|^4_{\mathrm{L}^4(\mathbb{S}^1)}, \end{aligned} \tag{2.14}$$

through the conservativity of $F_4(\boldsymbol{u})$ given in Theorem 2.1. Now making use of the Gagliardo–Nirenberg interpolation inequality there exists a constant C_{GN} such that

$$\|\boldsymbol{u}\|_{\mathrm{L}^4(\mathbb{S}^1)} \leq C_{GN}\|\boldsymbol{u}\|^{3/4}_{\mathrm{L}^2(\mathbb{S}^1)}\|\boldsymbol{u}_x\|^{1/4}_{\mathrm{L}^2(\mathbb{S}^1)}, \tag{2.15}$$

hence

$$\begin{aligned} \frac{1}{4}\|\boldsymbol{u}\|^4_{\mathrm{L}^4(\mathbb{S}^1)} &\leq \frac{1}{4}C_{GN}^4\|\boldsymbol{u}\|^3_{\mathrm{L}^2(\mathbb{S}^1)}\|\boldsymbol{u}_x\|_{\mathrm{L}^2(\mathbb{S}^1)} \\ &\leq \frac{1}{32}C_{GN}^8\|\boldsymbol{u}\|^6_{\mathrm{L}^2(\mathbb{S}^1)} + \frac{1}{2}\|\boldsymbol{u}_x\|^2_{\mathrm{L}^2(\mathbb{S}^1)}, \end{aligned} \tag{2.16}$$

through Young's inequality. Substituting (2.16) into (2.14) we see

$$\begin{aligned} \frac{1}{2}\|\boldsymbol{u}_x\|^2_{\mathrm{L}^2(\mathbb{S}^1)} &\leq 2F_4(\boldsymbol{u}_0) + \frac{C_{GN}^8}{32}\|\boldsymbol{u}\|^6_{\mathrm{L}^2(\mathbb{S}^1)} \\ &\leq 2F_4(\boldsymbol{u}_0) + \frac{C_{GN}^8}{4}F_2(\boldsymbol{u})^3 \\ &\leq 2F_4(\boldsymbol{u}_0) + \frac{C_{GN}^8}{4}F_2(\boldsymbol{u}_0)^3 \\ &\leq 2C_4 + \frac{C_{GN}^8 C_2^3}{4}, \end{aligned} \tag{2.17}$$

using the conservativity of $F_2(\boldsymbol{u})$, concluding the proof. $\square$

2.4 Remark *(Hierarchy of conservation laws).* Note that the vmKdV equation (2.2) admits an infinite hierarchy of conserved quantities. For example, after $F_2(\boldsymbol{u})$ and $F_4(\boldsymbol{u})$ the next member of the hierarchy is

$$F_6(\boldsymbol{u}) = \int_{S^1} \frac{1}{2}|\boldsymbol{u}|^6 + 10\,(\boldsymbol{u}\cdot\boldsymbol{u}_x)^2 + |\boldsymbol{u}|^2\,|\boldsymbol{u}_x|^2 + 7\,|\boldsymbol{u}|^2\,(\boldsymbol{u}\cdot\boldsymbol{u}_{xx}) + 4\,|\boldsymbol{u}_{xx}|^2\,\mathrm{d}x. \tag{2.18}$$

Together with the Gagliardo–Nirenberg interpolation inequality one may derive a priori bounds of a similar form to that given in Theorem 2.3 but in higher order norms. Indeed, for $s \in \mathbb{N}$ the conservation law F_{2s} naturally gives rise to a stability bound in H^{s-1}.

2.5 Remark *(Stability for a vmKdV-type problem).* The vmKdV-type equation given by

$$\boldsymbol{u}_t - \frac{3}{2}\boldsymbol{u}\cdot\boldsymbol{u}\boldsymbol{u}_x + \boldsymbol{u}_{xxx} = \boldsymbol{0} \tag{2.19}$$

forms an interesting alternative equation of study to the vmKdV equation (2.2). The reason is that the Hamiltonian is sign definite, that is

$$F_4(\boldsymbol{u}) := \int_{\mathbb{S}^1} \frac{1}{2}|\boldsymbol{u}_x|^2 + \frac{1}{8}|\boldsymbol{u}|^4 = \frac{1}{2}\|\boldsymbol{u}_x\|^2_{\mathrm{L}^2(\mathbb{S}^1)} + \frac{1}{8}\|\boldsymbol{u}\|^4_{\mathrm{L}^4(\mathbb{S}^1)}\,\mathrm{d}x, \tag{2.20}$$

hence the conservation of invariant immediately implies that, for any $t > 0$,

$$\frac{1}{2}\|\boldsymbol{u}_x(t)\|^2_{\mathrm{L}^2(\mathbb{S}^1)} + \frac{1}{8}\|\boldsymbol{u}(t)\|^4_{\mathrm{L}^4(\mathbb{S}^1)} = \frac{1}{2}\|\boldsymbol{u}_x(0)\|^2_{\mathrm{L}^2(\mathbb{S}^1)} + \frac{1}{8}\|\boldsymbol{u}(0)\|^4_{\mathrm{L}^4(\mathbb{S}^1)}, \tag{2.21}$$

guaranteeing stability of solutions without the necessity of the interpolation arguments of Proposition 2.3. We expect that the space of exact solutions to these two equations are quite different and leave the quantification of solutions of this problem for future work. In this work we will focus on (2.2), the structure of solutions to this problem and their numerical approximation.

2.6. Exact solutions to the vmKdV system

The vmKdV equation (2.2) is integrable and has already drawn some attention [3]. Its integrability properties were derived using the structure equation for the evolution of a curve embedded in an n-dimensional Riemannian manifold with constant curvature [39,2,30]. The associated Cauchy problem can be studied analytically using the inverse scattering transform [1,32,16]. Due to the fact that it admits a zero curvature representation (or a Lax representation, see [27, cf.]), i.e., it can be written in the following form:

$$U_t - V_x + [U, V] = 0, \tag{2.22}$$

where $U = U(\boldsymbol{u};\lambda)$ and $V = V(\boldsymbol{u};\lambda)$ are appropriate matrices in a Lie algebra having a polynomial dependence on a spectral parameter $\lambda \in \mathbb{C}$. One can construct a Darboux matrix M [36,38] that maps the pair (U, V) to

$$(U, V) \mapsto (\widetilde{U}, \widetilde{V}) = (MUM^{-1} + M_xM^{-1}, MUM^{-1} + M_tM^{-1}) \tag{2.23}$$

and $\widetilde{U} = U(\widetilde{\boldsymbol{u}};\lambda)$ and $\widetilde{V} = V(\widetilde{\boldsymbol{u}};\lambda)$. In other words $\widetilde{U}$ and $\widetilde{V}$ have the same structure as U and V respectively. The transformation (2.23) implies a nonlocal symmetry $\boldsymbol{u} \mapsto \widetilde{\boldsymbol{u}}$ of the vmKdV, known as a Bäcklund transformation. Such transformations that have applications in geometry [36] are characteristic of integrable equations. Starting with the trivial background solution $\boldsymbol{u} = \boldsymbol{0}$ one can then recursively and algebraically construct the soliton solutions of vmKdV equation (2.2). For example, when $d = 2$ a 1-soliton solution is given by

$$\boldsymbol{u} = \frac{2\mu}{\cosh\xi_\mu}\boldsymbol{E}, \tag{2.24}$$

where $\mu \in \mathbb{R}$, $\xi_\mu = \mu\left(x - c_\mu\right) - \mu^3 t$, for some shift $c_\mu \in \mathbb{R}$ and $\boldsymbol{E}$ is a constant unit vector. A 2-soliton solution is given by

$$\boldsymbol{u} = \frac{F_{\mu,\nu}}{G}\boldsymbol{E}_1 + \frac{F_{\nu,\mu}}{G}\boldsymbol{E}_2, \tag{2.25}$$

where $\boldsymbol{E}_1$ and $\boldsymbol{E}_2$ are constant unit vectors, $\mu,\ \nu \in \mathbb{R}$ with $\mu \neq \pm\nu$ and

$$F_{k,l} = 2(l^2 - k^2)l\cosh\xi_k \tag{2.26}$$

and

$$G = (\mu^2 + \nu^2)\cosh\xi_\mu \cosh\xi_\nu - 2\mu\nu \sinh\xi_\mu \sinh\xi_\nu - 2\mu\nu \boldsymbol{E}_1 \cdot \boldsymbol{E}_2. \tag{2.27}$$

The 1-soliton (2.24) and 2-soliton (2.25) solutions, while elegant, are not the most general of their kind. Nevertheless, the exact solutions (2.24) and (2.25) are both perfectly adequate for benchmarking our scheme which we shall use them for in §5. Such solutions can also be derived using Hirota's bilinear form [22,3].

Solitons are, however, a special class of solution for this problem with a very particular structure. In general one cannot write down closed form solutions for this problem motivating the need for long time accurate numerical schemes. We shall proceed by describing the Hamiltonian structure of the vmKdV problem which forms the basis for the design of our numerical scheme.

2.7 Remark *(Problem reformulation and motivation).* The vmKdV system is Hamiltonian and thus it can be written as

$$\boldsymbol{u}_t = \mathscr{P}(\boldsymbol{u}) \frac{\delta F_4(\boldsymbol{u})}{\delta \boldsymbol{u}}, \tag{2.28}$$

where $\mathscr{P}(\boldsymbol{u})$ is a Hamiltonian operator, $F_4(\boldsymbol{u})$ is the corresponding Hamiltonian and $\frac{\delta \cdot}{\delta \boldsymbol{u}}$ denotes the first variation with respect to $\boldsymbol{u}$ [33]. For this specific problem the Hamiltonian operator acts on a real, d-vector function $\boldsymbol{y}$ and takes the form [2]

$$\mathscr{P}(\boldsymbol{u})\boldsymbol{y} := \boldsymbol{y}_x - \boldsymbol{u} \lrcorner \left[\mathrm{D}_x^{-1} \left(\boldsymbol{y} \otimes \boldsymbol{u} - \boldsymbol{u} \otimes \boldsymbol{y} \right) \right], \tag{2.29}$$

where D_x^{-1} is the formal inverse operator of D_x, $\otimes$ is the tensor product between vectors and $\lrcorner$ is a product defined through

$$\boldsymbol{x} \lrcorner (\boldsymbol{y} \otimes \boldsymbol{z}) = (\boldsymbol{x} \cdot \boldsymbol{y})\, \boldsymbol{z}. \tag{2.30}$$

This then induces a *Poisson bracket*

$$\{F, G\} := \int_{\mathbb{R}} \frac{\delta F}{\delta u} \mathscr{P}(\boldsymbol{u}) \frac{\delta G}{\delta u} \, \mathrm{d}x, \tag{2.31}$$

a skew-symmetric bilinear form satisfying the Jacobi identity. In view of the skew-symmetry of $\mathscr{P}(\boldsymbol{u})$ we have

$$\mathrm{D}_t F_4(\boldsymbol{u}) = \{F_4(\boldsymbol{u}), F_4(\boldsymbol{u})\} = 0. \tag{2.32}$$

Notice also that the vmKdV system can also be written as

$$\boldsymbol{u}_t = \{\boldsymbol{u}, F_4(\boldsymbol{u})\}. \tag{2.33}$$

The main idea behind the discretisation we propose is to correctly *represent the Hamiltonian operator in the finite element space whilst preserving the skew-symmetry property of the underlying bracket*. Indeed, the proof of Proposition 2.1 motivates rewriting the vmKdV system by introducing auxiliary variables to represent different components of the Hamiltonian operator. We consider seeking the tuple $(\boldsymbol{u}, \boldsymbol{v}, \boldsymbol{w})$ such that

$$\begin{aligned} \boldsymbol{0} &= \boldsymbol{u}_t + \boldsymbol{v}_x + \boldsymbol{w} \\ \boldsymbol{0} &= \boldsymbol{v} - \frac{1}{2} |\boldsymbol{u}|^2 \boldsymbol{u} - \boldsymbol{u}_{xx} \\ \boldsymbol{0} &= \boldsymbol{w} - |\boldsymbol{u}|^2 \boldsymbol{u}_x + (\boldsymbol{u}_x \cdot \boldsymbol{u})\, \boldsymbol{u}. \end{aligned} \tag{2.34}$$

Notice that $\boldsymbol{v} = \frac{\delta F_4(\boldsymbol{u})}{\delta u}$ and $\boldsymbol{w} = \boldsymbol{u} \lrcorner \left[\mathrm{D}_x^{-1} \left(\boldsymbol{v} \otimes \boldsymbol{u} - \boldsymbol{u} \otimes \boldsymbol{v} \right) \right]$. This form of $\boldsymbol{w}$ is extremely important as the Hamiltonian operator given in (2.29) is nonlocal. The fact that it can be "localised" by removing the D_x^{-1} allows for the efficient approximation by Galerkin methods.

This reformulation also means that in the case both arguments of the Poisson bracket are the Hamiltonian we may write

$$0 = \{F_4(\boldsymbol{u}), F_4(\boldsymbol{u})\} = \int_{\mathbb{R}} \boldsymbol{v} \cdot (\boldsymbol{v}_x + \boldsymbol{w}) \, \mathrm{d}x. \tag{2.35}$$

It is exactly this structure that we try to exploit.

2.8 Remark *(Relation to the scalar case).* As already mentioned when $d = 1$, the problem reduces to the mKdV equation. In this case $w \equiv 0$ and the mixed system coincides with that proposed in [24]. Energy conservative schemes can be derived and proven to converge using the same techniques presented in that work. For $d > 1$, $\boldsymbol{w}$ is not necessarily zero and represents the additional contribution arising from the Hamiltonian operator described in Remark 2.7.

2.9 Proposition *(The mixed system is conservative). Let $\boldsymbol{u}$, $\boldsymbol{v}$, $\boldsymbol{w}$ be given by (2.34) then we have that*

$$\mathrm{D}_t F_4(\boldsymbol{u}) = \mathrm{D}_t \int_{\mathbb{S}^1} \frac{1}{2} |\boldsymbol{u}_x|^2 - \frac{1}{8} |\boldsymbol{u}|^4 \, \mathrm{d}x = 0. \tag{2.36}$$

Proof. Since the mixed system is equivalent to the vmKdV system the proof is clear through Proposition 2.1, however, for illustrative purposes we present it in full as it will become the basis for the design of our numerical scheme. To begin note

$$\begin{aligned} \mathrm{D}_t F_4(\boldsymbol{u}) &= \int_{\mathbb{S}^1} \boldsymbol{u}_x \cdot \boldsymbol{u}_{xt} - \frac{1}{2} |\boldsymbol{u}|^2 \boldsymbol{u} \cdot \boldsymbol{u}_t \, \mathrm{d}x \\ &= \int_{\mathbb{S}^1} -\boldsymbol{u}_{xx} \cdot \boldsymbol{u}_t - \frac{1}{2} |\boldsymbol{u}|^2 \boldsymbol{u} \cdot \boldsymbol{u}_t \, \mathrm{d}x \\ &= \int_{\mathbb{S}^1} -\boldsymbol{v} \cdot \boldsymbol{u}_t \, \mathrm{d}x. \end{aligned} \tag{2.37}$$

Now making use of (2.34)

$$\begin{aligned} \mathrm{D}_t F_4(\boldsymbol{u}) &= \int_{\mathbb{S}^1} \boldsymbol{v} \cdot (\boldsymbol{v}_x + \boldsymbol{w}) \, \mathrm{d}x \\ &= \int_{\mathbb{S}^1} \boldsymbol{v} \cdot \boldsymbol{w} \, \mathrm{d}x \\ &= \int_{\mathbb{S}^1} \left(\frac{1}{2} |\boldsymbol{u}|^2 \boldsymbol{u} + \boldsymbol{u}_{xx} \right) \cdot \boldsymbol{w} \, \mathrm{d}x. \end{aligned} \tag{2.38}$$

Note that from (2.34) we can see that $\boldsymbol{w} \cdot \boldsymbol{u} = 0$ and hence

$$\begin{aligned} \mathrm{D}_t F_4(\boldsymbol{u}) &= \int_{\mathbb{S}^1} \boldsymbol{u}_{xx} \cdot \boldsymbol{w} \, \mathrm{d}x \\ &= \int_{\mathbb{S}^1} \boldsymbol{u}_{xx} \cdot \left(|\boldsymbol{u}|^2 \boldsymbol{u}_x - (\boldsymbol{u}_x \cdot \boldsymbol{u}) \boldsymbol{u} \right) \mathrm{d}x. \end{aligned} \tag{2.39}$$

Now, through an integration by parts we have

$$\begin{aligned} \int_{\mathbb{S}^1} |\boldsymbol{u}|^2 \boldsymbol{u}_x \cdot \boldsymbol{u}_{xx} &= -\int_{\mathbb{S}^1} \left(|\boldsymbol{u}|^2 \boldsymbol{u}_x \right)_x \cdot \boldsymbol{u}_x \\ &= -\int_{\mathbb{S}^1} 2 (\boldsymbol{u} \cdot \boldsymbol{u}_x) (\boldsymbol{u}_x \cdot \boldsymbol{u}_x) + |\boldsymbol{u}|^2 \boldsymbol{u}_{xx} \cdot \boldsymbol{u}_x \, \mathrm{d}x \end{aligned} \tag{2.40}$$

and hence

$$\int_{\mathbb{S}^1} |\boldsymbol{u}|^2 \boldsymbol{u}_x \cdot \boldsymbol{u}_{xx} = -\int_{\mathbb{S}^1} (\boldsymbol{u} \cdot \boldsymbol{u}_x) (\boldsymbol{u}_x \cdot \boldsymbol{u}_x). \tag{2.41}$$

In addition,

$$\begin{aligned} \int_{\mathbb{S}^1} (\boldsymbol{u}_x \cdot \boldsymbol{u}) (\boldsymbol{u} \cdot \boldsymbol{u}_{xx}) \, \mathrm{d}x &= -\int_{\mathbb{S}^1} (\boldsymbol{u}_x \cdot \boldsymbol{u}\boldsymbol{u})_x \cdot \boldsymbol{u}_x \, \mathrm{d}x \\ &= -\int_{\mathbb{S}^1} (\boldsymbol{u}_{xx} \cdot \boldsymbol{u}) (\boldsymbol{u} \cdot \boldsymbol{u}_x) + 2 (\boldsymbol{u}_x \cdot \boldsymbol{u}_x) (\boldsymbol{u} \cdot \boldsymbol{u}_x) \, \mathrm{d}x \end{aligned} \tag{2.42}$$

and hence

$$\int_{\mathbb{S}^1} (\boldsymbol{u}_x \cdot \boldsymbol{u})\,(\boldsymbol{u} \cdot \boldsymbol{u}_{xx})\,\mathrm{d}x = -\int_{\mathbb{S}^1} (\boldsymbol{u}_x \cdot \boldsymbol{u}_x)\,(\boldsymbol{u} \cdot \boldsymbol{u}_x)\,\mathrm{d}x. \tag{2.43}$$

Substituting (2.41) and (2.43) into (2.39) concludes the proof. □

3. Temporal discretisation

For the readers convenience we will present an argument for designing the temporally discrete scheme in the spatially continuous setting. We consider a time interval $[0, T]$ subdivided into a partition of N consecutive adjacent subintervals whose endpoints are denoted $t_0 = 0 < t_1 < \ldots < t_N = T$. The n-th timestep is defined as $\tau_n := t_{n+1} - t_n$. We will consistently use the shorthand $y^n(\cdot) := y(\cdot, t_n)$ for a generic time function y. We also denote $y^{n+\frac{1}{2}} := \frac{1}{2}\left(y^n + y^{n+1}\right)$.

We consider the temporal discretisation of the mixed system (2.34) as follows: Given $\boldsymbol{u}^0$, for $n \in [0, N]$ find $\boldsymbol{u}^{n+1}$ such that

$$\begin{aligned}
\boldsymbol{0} &= \frac{\boldsymbol{u}^{n+1} - \boldsymbol{u}^n}{\tau_n} + \boldsymbol{v}_x^{n+1} + \boldsymbol{w}^{n+1} \\
\boldsymbol{0} &= \boldsymbol{v}^{n+1} - \frac{1}{2}\left(\left|\boldsymbol{u}^n\right|^2 + \left|\boldsymbol{u}^{n+1}\right|^2\right)\boldsymbol{u}^{n+\frac{1}{2}} - \boldsymbol{u}_{xx}^{n+\frac{1}{2}} \\
\boldsymbol{0} &= \boldsymbol{w}^{n+1} - \left|\boldsymbol{u}^{n+\frac{1}{2}}\right|^2 \boldsymbol{u}_x^{n+\frac{1}{2}} + \left(\boldsymbol{u}_x^{n+\frac{1}{2}} \cdot \boldsymbol{u}^{n+\frac{1}{2}}\right)\boldsymbol{u}^{n+\frac{1}{2}}.
\end{aligned} \tag{3.1}$$

3.1 Remark *(Structure of the temporal discretisation).* The temporal discretisation given in (3.1) is *not* a Runge–Kutta method. It resembles a Crank–Nicolson discretisation, however the treatment of the nonlinearity is different. It is formally of second order and is constructed such that it satisfies the next Theorem. Although construction of higher order methods is possible they become very complicated to write down so we will not press this point here.

3.2 Theorem *(Conservativity of the temporal discretisation). Let $\{\boldsymbol{u}^n\}_{n=0}^N$ be a temporally discrete solution of (3.1) then we have*

$$F_4(\boldsymbol{u}^n) = F_4(\boldsymbol{u}^0) \quad \forall\, n \in [0, N]. \tag{3.2}$$

Proof. It suffices to show that

$$F_4(\boldsymbol{u}^{n+1}) - F_4(\boldsymbol{u}^n) = 0 \tag{3.3}$$

and then the result follows inductively. So

$$\begin{aligned}
2\left(F_4(\boldsymbol{u}^{n+1}) - F_4(\boldsymbol{u}^n)\right) &= \int_{\mathbb{S}^1} \left|\boldsymbol{u}_x^{n+1}\right|^2 - \left|\boldsymbol{u}_x^n\right|^2 - \frac{1}{4}\left|\boldsymbol{u}^{n+1}\right|^4 + \frac{1}{4}\left|\boldsymbol{u}^n\right|^4 \mathrm{d}x \\
&= \int_{\mathbb{S}^1} \left(\boldsymbol{u}_x^{n+1} - \boldsymbol{u}_x^n\right) \cdot \left(\boldsymbol{u}_x^{n+1} + \boldsymbol{u}_x^n\right) \\
&\quad - \frac{1}{4}\left(\boldsymbol{u}^{n+1} - \boldsymbol{u}^n\right) \cdot \left(\left|\boldsymbol{u}^{n+1}\right|^2 \boldsymbol{u}^{n+1} + \left|\boldsymbol{u}^{n+1}\right|^2 \boldsymbol{u}^n + \left|\boldsymbol{u}^n\right|^2 \boldsymbol{u}^{n+1} + \left|\boldsymbol{u}^n\right|^2 \boldsymbol{u}^n\right) \mathrm{d}x \\
&= -\int_{\mathbb{S}^1} \left(\boldsymbol{u}^{n+1} - \boldsymbol{u}^n\right) \cdot \left(\boldsymbol{u}_{xx}^{n+1} + \boldsymbol{u}_{xx}^n\right) \\
&\quad - \frac{1}{2}\left(\boldsymbol{u}^{n+1} - \boldsymbol{u}^n\right) \cdot \left(\left|\boldsymbol{u}^{n+1}\right|^2 \boldsymbol{u}^{n+\frac{1}{2}} + \left|\boldsymbol{u}^n\right|^2 \boldsymbol{u}^{n+\frac{1}{2}}\right) \mathrm{d}x \\
&= -\int_{\mathbb{S}^1} \left(\boldsymbol{u}^{n+1} - \boldsymbol{u}^n\right) \cdot \boldsymbol{v}^{n+1}\,\mathrm{d}x,
\end{aligned} \tag{3.4}$$

through expanding differences, integrating by parts and using the scheme (3.1). Now, again using the scheme

$$
\begin{aligned}
2\left(F_4(\boldsymbol{u}^{n+1}) - F_4(\boldsymbol{u}^n)\right) &= \int_{\mathbb{S}^1} \tau_n \left(\boldsymbol{v}_x^{n+1} + \boldsymbol{w}^{n+1}\right) \cdot \boldsymbol{v}^{n+1} \,\mathrm{d}x \\
&= \int_{\mathbb{S}^1} \tau_n \boldsymbol{w}^{n+1} \cdot \boldsymbol{v}^{n+1} \,\mathrm{d}x \\
&= \int_{\mathbb{S}^1} \tau_n \boldsymbol{w}^{n+1} \cdot \left(\frac{1}{2}\left(\left|\boldsymbol{u}^{n+1}\right|^2 \boldsymbol{u}^{n+\frac{1}{2}} + \left|\boldsymbol{u}^{n}\right|^2 \boldsymbol{u}^{n+\frac{1}{2}}\right) + \boldsymbol{u}_{xx}^{n+\frac{1}{2}}\right) \mathrm{d}x \\
&= \int_{\mathbb{S}^1} \tau_n \boldsymbol{w}^{n+1} \cdot \boldsymbol{u}_{xx}^{n+\frac{1}{2}} \,\mathrm{d}x,
\end{aligned}
\tag{3.5}
$$

in view of the orthogonality condition $\boldsymbol{w}^{n+1} \cdot \boldsymbol{u}^{n+\frac{1}{2}} = 0$ following from the third equation of (3.1). Now we may use the definition of $\boldsymbol{w}^{n+1}$ and the identities (2.41) and (2.43) to conclude. □

3.3 Remark *(Conservation of other invariants).* This discretisation does not lend itself to conservation of other invariants, for example even the quadratic invariant F_2 is not conserved under this scheme. A class of Runge–Kutta methods that are able to exactly conserve all quadratic invariants are the Gauss–Radau family, this is because they are *symplectic*. When one considers higher order invariants, it seems that schemes must be designed individually and there is no class that can exactly conserve all.

4. Spatial and full discretisation

In this section we describe the discretisation which we analyse for the approximation of (2.2). We show that the scheme has a constant energy functional consistent with that of the original PDE system.

4.1 Definition *(Finite element space).* We discretise (2.2) spatially using a piecewise polynomial continuous finite element method. To that end we let $\mathbb{S}^1 := [0, 1]$ be the unit interval with matching endpoints and choose

$$0 = x_0 < x_1 < \cdots < x_M = 1. \tag{4.1}$$

Note that in the numerical experiments we take a larger periodic interval, however for clarity of presentation we restrict our attention in this section to $\mathbb{S}^1$. We denote $K_m = [x_m, x_{m+1}]$ to be the m-th subinterval and let $h_m := |K_m|$ be its length with $\mathscr{T} = \{K_m\}_{m=0}^{M-1}$. We impose that the ratio h_m/h_{m+1} is bounded from above and below for $m = 0, \ldots, M-1$. Let $\mathbb{P}^q$ be the space of polynomials of degree less than or equal to q, then we introduce the *finite element space*

$$\mathbb{V} := \left\{\Phi : \ \Phi|_{K_m} \in \mathbb{P}^q(K_m) \cap \mathrm{C}^0(\mathbb{S}^1)\right\}. \tag{4.2}$$

Throughout this section and in the sequel, we will use capital Latin letters to denote spatially discrete trial functions and capital Greek letters to denote discrete test functions.

4.2. Spatial discretisation

Before we give the discretisation let us first consider a direct semi-discretisation of the mixed system (2.34), to find $(\boldsymbol{U}, \boldsymbol{V}, \boldsymbol{W}) \in \mathbb{V}^d \times \mathbb{V}^d \times \mathbb{V}^d$ such that

$$
\begin{aligned}
0 &= \int_{\mathbb{S}^1} (\boldsymbol{U}_t + \boldsymbol{V}_x + \boldsymbol{W}) \cdot \boldsymbol{\Phi} \,\mathrm{d}x \\
0 &= \int_{\mathbb{S}^1} \left(\boldsymbol{V} - \frac{1}{2}|\boldsymbol{U}|^2 \boldsymbol{U}\right) \cdot \boldsymbol{\Psi} + \boldsymbol{U}_x \cdot \boldsymbol{\Psi}_x \,\mathrm{d}x \\
0 &= \int_{\mathbb{S}^1} \left(\boldsymbol{W} - |\boldsymbol{U}|^2 \boldsymbol{U}_x + (\boldsymbol{U}_x \cdot \boldsymbol{U})\boldsymbol{U}\right) \cdot \boldsymbol{\Xi} \,\mathrm{d}x \quad \forall\ (\boldsymbol{\Phi}, \boldsymbol{\Psi}, \boldsymbol{\Xi}) \in \mathbb{V}^d \times \mathbb{V}^d \times \mathbb{V}^d.
\end{aligned}
\tag{4.3}
$$

One may run through the calculation in the Proof of Proposition 2.9 analogously to see that

$$\mathrm{D}_t F_4(\boldsymbol{U}) = \int_{\mathbb{S}^1} \boldsymbol{V} \cdot \boldsymbol{W} \,\mathrm{d}x, \tag{4.4}$$

whereby in the continuous case one uses the fact that $\boldsymbol{v}$ and $\boldsymbol{w}$ are orthogonal. In the discrete setting there is no reason why this should be the case and, indeed, except in very special cases, it is not. This necessitates a formulation that forces $\int_{\mathbb{S}^1} \boldsymbol{V} \cdot \boldsymbol{W} \, \mathrm{d}x = 0$ thus ensuring conservation of $F_4(\boldsymbol{U})$. We achieve this through a Lagrange multiplier approach encapsulated by the following spatially discrete scheme, to seek $(\boldsymbol{U}, \boldsymbol{V}, \boldsymbol{W}, P) \in \mathbb{V}^d \times \mathbb{V}^d \times \mathbb{V}^d \times \mathbb{R}/\{0\}$ such that

$$\begin{aligned}
0 &= \int_{\mathbb{S}^1} (\boldsymbol{U}_t + \boldsymbol{V}_x + \boldsymbol{W}) \cdot \boldsymbol{\Phi} \, \mathrm{d}x \\
0 &= \int_{\mathbb{S}^1} \left(\boldsymbol{V} - \frac{1}{2} |\boldsymbol{U}|^2 \boldsymbol{U} \right) \cdot \boldsymbol{\Psi} + \boldsymbol{U}_x \cdot \boldsymbol{\Psi}_x \, \mathrm{d}x \\
0 &= \int_{\mathbb{S}^1} \left(\boldsymbol{W} - |\boldsymbol{U}|^2 \boldsymbol{U}_x + (\boldsymbol{U}_x \cdot \boldsymbol{U}) \boldsymbol{U} \right) \cdot \boldsymbol{\Xi} \, \mathrm{d}x \\
0 &= \int_{\mathbb{S}^1} P \boldsymbol{V} \cdot \boldsymbol{\Xi} + \boldsymbol{V} \cdot \boldsymbol{W} \, \Pi \, \mathrm{d}x \\
\boldsymbol{U}^0 &= I^0 u_0, \quad \forall \ (\boldsymbol{\Phi}, \boldsymbol{\Psi}, \boldsymbol{\Xi}, \Pi) \in \mathbb{V}^d \times \mathbb{V}^d \times \mathbb{V}^d \times \mathbb{R}/\{0\}
\end{aligned} \tag{4.5}$$

4.3 Theorem *(Conservativity of the spatially discrete scheme). Let* $(\boldsymbol{U}, \boldsymbol{V}, \boldsymbol{W}, P)$ *solve the spatially discrete formulation (4.5) then*

$$\mathrm{D}_t F_4(\boldsymbol{U}) = \mathrm{D}_t \int_{\mathbb{S}^1} \frac{1}{2} |\boldsymbol{U}_x|^2 - \frac{1}{8} |\boldsymbol{U}|^4 \, \mathrm{d}x = 0. \tag{4.6}$$

Proof. An analogous argument to the Proof of Proposition 2.9 yields (4.4). To conclude pick $\Pi = P$ and $\boldsymbol{\Xi} = \boldsymbol{W}$ to see that

$$2P \int_{\mathbb{S}^1} \boldsymbol{V} \cdot \boldsymbol{W} \, \mathrm{d}x = 0, \tag{4.7}$$

as required. □

4.4 Remark *(Compatibility of the scheme with the Poisson bracket).* Notice that in view of Theorem 4.3 the spatial discretisation is compatible with the Poisson structure of the vmKdV system, indeed, using the same formulation as (2.35) we have that the numerical scheme can be written as

$$\boldsymbol{U}_t = \{\boldsymbol{U}, \boldsymbol{F}_4(\boldsymbol{U})\} = -\left(\pi\left(\boldsymbol{V}_x\right) + \boldsymbol{W}\right), \tag{4.8}$$

where π denotes the L^2 orthogonal projector onto $\mathbb{V}$. In addition, the evolution of the Hamiltonian can be described consistently

$$\mathrm{D}_t F_4(\boldsymbol{U}) = \{F_4(\boldsymbol{U}), F_4(\boldsymbol{U})\} = 0. \tag{4.9}$$

It is important to note that the evolution of other quantities, such as further invariants are not compatible with this structure, for example

$$\mathrm{D}_t F_2(\boldsymbol{U}) = \{F_2(\boldsymbol{U}), F_4(\boldsymbol{U})\} \neq 0. \tag{4.10}$$

4.5 Remark *(Discrete stability for the vmKdV-type problem).* Applying the same numerical discretisation techniques to the vmKdV-type equation (2.19) results in the spatially discrete numerical scheme to seek $(\boldsymbol{U}, \boldsymbol{V}, \boldsymbol{W}, P) \in \mathbb{V}^d \times \mathbb{V}^d \times \mathbb{V}^d \times \mathbb{R}/\{0\}$ such that

$$\begin{aligned}
0 &= \int_{\mathbb{S}^1} (\boldsymbol{U}_t + \boldsymbol{V}_x + \boldsymbol{W}) \cdot \boldsymbol{\Phi} \, \mathrm{d}x \\
0 &= \int_{\mathbb{S}^1} \left(\boldsymbol{V} + \frac{1}{2} |\boldsymbol{U}|^2 \boldsymbol{U} \right) \cdot \boldsymbol{\Psi} + \boldsymbol{U}_x \cdot \boldsymbol{\Psi}_x \, \mathrm{d}x \\
0 &= \int_{\mathbb{S}^1} \left(\boldsymbol{W} + |\boldsymbol{U}|^2 \boldsymbol{U}_x - (\boldsymbol{U}_x \cdot \boldsymbol{U}) \boldsymbol{U} \right) \cdot \boldsymbol{\Xi} \, \mathrm{d}x
\end{aligned} \tag{4.11}$$

$$0 = \int_{\mathbb{S}^1} P\boldsymbol{V}\cdot\boldsymbol{\Xi} + \boldsymbol{V}\cdot\boldsymbol{W}\,\Pi\,\mathrm{d}x$$
$$\boldsymbol{U}^0 = I^0 u_0, \quad \forall\ (\boldsymbol{\Phi},\boldsymbol{\Psi},\boldsymbol{\Xi},\Pi)\in\mathbb{V}^d\times\mathbb{V}^d\times\mathbb{V}^d\times\mathbb{R}/\{0\}$$

and we are then able to show for

$$\mathrm{D}_t F_4(\boldsymbol{U}) = \mathrm{D}_t\left(\frac{1}{2}\|\boldsymbol{U}_x\|^2_{\mathrm{L}^2(\mathbb{S}^1)} + \frac{1}{8}\|\boldsymbol{U}\|^4_{\mathrm{L}^4(\mathbb{S}^1)}\right) = 0, \tag{4.12}$$

guaranteeing, for any $t>0$,

$$\frac{1}{2}\|\boldsymbol{U}_x(t)\|^2_{\mathrm{L}^2(\mathbb{S}^1)} + \frac{1}{8}\|\boldsymbol{U}(t)\|^4_{\mathrm{L}^4(\mathbb{S}^1)} = \frac{1}{2}\|\boldsymbol{U}_x(0)\|^2_{\mathrm{L}^2(\mathbb{S}^1)} + \|\boldsymbol{U}(0)\|^4_{\mathrm{L}^4(\mathbb{S}^1)}. \tag{4.13}$$

4.6. Fully discrete scheme

Making use of the semi discretisations developed in §3 and §4 we consider a fully discrete approximation that consists of finding a sequence of functions $\left(\boldsymbol{U}^{n+1},\boldsymbol{V}^{n+1},\boldsymbol{W}^{n+1},P^{n+1}\right)\in[\mathbb{V}^n]^d\times[\mathbb{V}^n]^d\times[\mathbb{V}^n]^d\times\mathbb{R}/\{0\}$ such that for each $n\in[0,N-1]$ we have

$$\begin{aligned}
0 &= \int_{\mathbb{S}^1}\left(\frac{\boldsymbol{U}^{n+1}-\boldsymbol{U}^n}{\tau_n} + \boldsymbol{V}^{n+1}_x + \boldsymbol{W}^{n+1}\right)\cdot\boldsymbol{\Phi}\,\mathrm{d}x\\
0 &= \int_{\mathbb{S}^1}\left(\boldsymbol{V}^{n+1} - \frac{1}{2}\left(\left|\boldsymbol{U}^n\right|^2 + \left|\boldsymbol{U}^{n+1}\right|^2\right)\boldsymbol{U}^{n+1/2}\right)\cdot\boldsymbol{\Psi} + \boldsymbol{U}^{n+1/2}_x\cdot\boldsymbol{\Psi}_x\,\mathrm{d}x\\
0 &= \int_{\mathbb{S}^1}\left(\boldsymbol{W}^{n+1} - \left|\boldsymbol{U}^{n+1/2}\right|^2\boldsymbol{U}^{n+1/2}_x + \left(\boldsymbol{U}^{n+1/2}_x\cdot\boldsymbol{U}^{n+1/2}\right)\boldsymbol{U}^{n+1/2}\right)\cdot\boldsymbol{\Xi}\,\mathrm{d}x\\
0 &= \int_{\mathbb{S}^1} P^{n+1}\boldsymbol{V}^{n+1}\cdot\boldsymbol{\Xi} + \boldsymbol{V}^{n+1}\cdot\boldsymbol{W}^{n+1}\,\Pi\,\mathrm{d}x\\
\boldsymbol{U}^0 &= \pi^0 u_0, \quad \forall\ (\boldsymbol{\Phi},\boldsymbol{\Psi},\boldsymbol{\Xi},\Pi)\in\left[\mathbb{V}^n\right]^d\times\left[\mathbb{V}^n\right]^d\times\left[\mathbb{V}^n\right]^d\times\mathbb{R}/\{0\}
\end{aligned} \tag{4.14}$$

where π^0 denotes the L^2 orthogonal projector into $\mathbb{V}^0$. This is the direct discretisation of the mixed system (2.34) with the temporal discretisation as that proposed in §3 with an additional equation for a unknown real number that represents a Lagrange multiplier ensuring $\int_{\mathbb{S}^1}\boldsymbol{V}^n\cdot\boldsymbol{W}^n\,\mathrm{d}x = 0$ for all n.

4.7 Theorem *(Conservativity of the fully discrete scheme). Let $\{\boldsymbol{U}^n\}_{n=0}^N$ be the fully discrete scheme generated by (4.14), then we have that*

$$F_4(\boldsymbol{U}^n) = F_4(\boldsymbol{U}^0) \quad \forall\, n\in[0,N]. \tag{4.15}$$

Proof. It suffices to show that

$$F_4(\boldsymbol{U}^{n+1}) - F_4(\boldsymbol{U}^n) = 0 \tag{4.16}$$

and then the result follows inductively. To this end

$$\begin{aligned}
2\left(F_4(\boldsymbol{U}^{n+1}) - F_4(\boldsymbol{U}^n)\right) &= \int_{\mathbb{S}^1}\left|\boldsymbol{U}^{n+1}_x\right|^2 - \left|\boldsymbol{U}^n_x\right|^2 - \frac{1}{4}\left|\boldsymbol{U}^{n+1}\right|^4 + \frac{1}{4}\left|\boldsymbol{U}^n\right|^4\,\mathrm{d}x\\
&= \int_{\mathbb{S}^1}\left(\boldsymbol{U}^{n+1}_x - \boldsymbol{U}^n_x\right)\cdot\left(\boldsymbol{U}^{n+1}_x + \boldsymbol{U}^n_x\right)\\
&\quad - \frac{1}{4}\left(\boldsymbol{U}^{n+1} - \boldsymbol{U}^n\right)\cdot\left(\left|\boldsymbol{U}^{n+1}\right|^2\boldsymbol{U}^{n+1} + \left|\boldsymbol{U}^{n+1}\right|^2\boldsymbol{U}^n + \left|\boldsymbol{U}^n\right|^2\boldsymbol{U}^{n+1} + \left|\boldsymbol{U}^n\right|^2\boldsymbol{U}^n\right)\mathrm{d}x\\
&= -\int_{\mathbb{S}^1}\left(\boldsymbol{U}^{n+1} - \boldsymbol{U}^n\right)\cdot\boldsymbol{V}^{n+1}\,\mathrm{d}x,
\end{aligned} \tag{4.17}$$

through expanding differences and using the second equation of (4.14). Now, using the first equation of (4.14)

$$\begin{aligned} 2\left(F_4(\boldsymbol{U}^{n+1}) - F_4(\boldsymbol{U}^n)\right) &= \int_{\mathbb{S}^1} \tau_n \left(\boldsymbol{V}_x^{n+1} + \boldsymbol{W}^{n+1}\right) \cdot \boldsymbol{V}^{n+1} \,\mathrm{d}x \\ &= \int_{\mathbb{S}^1} \tau_n \boldsymbol{W}^{n+1} \cdot \boldsymbol{V}^{n+1} \,\mathrm{d}x \\ &= 0 \end{aligned} \tag{4.18}$$

using the fourth equation of (4.14) with $\Pi = P^{n+1}$ and $\boldsymbol{\Xi} = \boldsymbol{W}^{n+1}$, concluding the proof. □

5. Numerical experiments

In this section we illustrate the performance of the method proposed through a series of numerical experiments. The brunt of the computational work has been carried out using Firedrake [34]. We employ a Gauss quadrature of order $4q$, where q is the degree of the finite element space, to minimise quadrature error introduced into the implementation. Indeed, at this degree all integrals are performed exactly with the exception of the projection of the initial condition. The nonlinear system of equations are then approximated using the PETSc [6,5] Newton line search method with a tolerance of 10^{-12} on each time step. A combination of Paraview and Matplotlib have been used as a visualisation tool. The code written for this purpose is freely available at [23]. For each benchmark test we fix the polynomial degree q and compute a sequence of solutions with $h = h(i) = 2^{-i}$ and τ chosen either so $\tau \ll h$, to make the temporal discretisation error negligible, or so $\tau = h$ so temporal discretisation error dominates. This is done for a sequence of refinement levels, $i = l, \dots, L$. We have previously used S^1 as the unitary periodic domain. For our numerical experiments, we have scaled the domain to [0,40] for computational convenience.

5.1 Definition *(Experimental order of convergence).* Given two sequences $a(i)$ and $h(i) \searrow 0$ we define the *experimental order of convergence* (EOC) to be the local slope of the $\log a(i)$ vs. $\log h(i)$ curve, i.e.,

$$\mathrm{EOC}(a, h; i) = \frac{\log\left(\frac{a(i+1)}{a(i)}\right)}{\log\left(\frac{h(i+1)}{h(i)}\right)}. \tag{5.1}$$

5.2 Remark *(Numerical deviation in F_4).* While the analysis shows that our scheme *exactly* preserves the energy over arbitrarily long time, the implementation relies on linear and nonlinear solvers that inherently require further approximation. The result of this is that the energy may deviate *locally* up to the tolerance of the linear and nonlinear solvers which introduces the possibility of these errors propagating over time. In our numerical tests we focus on studying the global deviation in time, $F_4(U^n) - F_4(U^0)$, which *includes* any propagation arising from solver or precision errors.

5.3. Test 1 – asymptotic benchmarking of a 1-soliton solution

We take $d = 2$ and

$$\boldsymbol{u_0} = \frac{2\mu}{\cosh\left(\mu\left(x - c_\mu\right)\right)}\boldsymbol{E}, \tag{5.2}$$

over the periodic domain S^1 with $\boldsymbol{E} = (0.8, (1 - 0.8^2)^{0.5})^\intercal$, $\mu = 1$ and $c_\mu = 20$. The exact solution is then given by (2.24). We take a uniform timestep and uniform meshes that are fixed with respect to time. Convergence results are shown in Fig. 2 and conservativity over long time is given in Fig. 1. Note that for the 1-soliton solution we have $\boldsymbol{W}^n \equiv \boldsymbol{0}$ for all n in which case the Lagrange multiplier is not required as $\int_{\mathbb{S}^1} \boldsymbol{V}^n \cdot \boldsymbol{W}^n = 0$ trivially for all n.

For this test case we also investigate how well the qualitative structure of the solution is captured. In the spirit of [9] we investigate the amplitude error, phase error and shape error of a single soliton over time. To that end, we define $\boldsymbol{X}$ as the set of Lagrange degrees of freedom for the partition $\mathscr{T}$.

The amplitude error for U_i is then given by

$$\max_{\boldsymbol{X}} U_i - \max_{\boldsymbol{X}} u_i. \tag{5.3}$$

If the amplitude error is positive then the numerical soliton is larger than the exact solution, and vice versa. Similarly we define the phase error as

$$e_{p_i} = \operatorname*{argmax}_{\boldsymbol{X}} U_i - \operatorname*{argmax}_{\boldsymbol{X}} u_i, \tag{5.4}$$

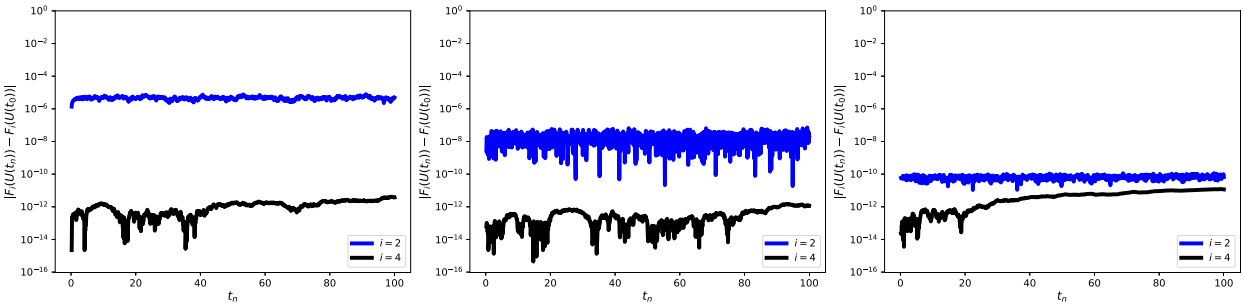

(a) Here $q = 1$. (b) Here $q = 2$. (c) Here $q = 3$.

Fig. 1. Here we examine the conservative discretisation scheme with various polynomial degrees, q, approximating the exact solution (2.24) with initial conditions given by (5.2). We show the deviation in the two invariants F_i, $i = 2, 4$, corresponding to momentum and energy. In each test we take a fixed spatial discretisation parameter of $h = 0.25$ and fixed time step of $\tau = 0.001$. Notice that in each case the deviation in energy is smaller than the solver tolerance of 10^{-12} and the deviation in momentum is bounded. In addition, as the degree of approximation is increased the deviation in momentum becomes smaller, in this case by around two orders of magnitude per polynomial order. The simulations are simulated for long time to test conservativity with $T = 100$ in each case. (For interpretation of the colours in the figure(s), the reader is referred to the web version of this article.)

where `argmax` represents the spatial coordinate associated to the maximum over $\boldsymbol{X}$. If the phase error is positive then the numerical approximation is moving faster than the exact solution, and vice versa. Note this discrete measure of the error cannot detect shifts in phase which are smaller than the distance between degrees of freedom. The amplitude and phase errors for this test case can be seen in Fig. 3 and Fig. 4 respectively.

In [9] the shape error is defined to be $\min_{y\in\mathbb{S}^1} \|u_i(x+y,t_n) - U_i(x,t_n)\|_{\mathrm{L}^2(\mathbb{S}^1)}$ in each vector component of the solution. Numerically we approximate this error by shifting the exact solution by the distance of the phase error and computing the L_2 error at fixed times, i.e., the discrete shape error is

$$\left\| u_i(x + e_{p_i}, t_n) - U_i(x, t_n) \right\|_{\mathrm{L}^2(\mathbb{S}^1)}.$$

The shape error for this test can be seen in Fig. 5.

5.4. Test 2 – asymptotic benchmarking of a 2-soliton solution

We take $d = 2$ and

$$\boldsymbol{u}_0 = \frac{F_{\mu,\nu}}{G}\boldsymbol{E}_1 + \frac{F_{\nu,\mu}}{G}\boldsymbol{E}_2, \tag{5.5}$$

with $F_{\mu,\nu}$ given in (2.26) G given in (2.27). The parameters are $\boldsymbol{E_1} = (1,0)^\intercal$, $\boldsymbol{E_2} = (0,1)^\intercal$, $\mu = \sqrt{2}$, $\nu = \sqrt{3}$, $c_\nu = 24.9$, $c_\mu = 25.1$. The exact solution is then given by 2.6. We take a uniform timestep and uniform meshes that are fixed with respect to time. Convergence results are shown in Fig. 7 and conservativity over long time is given in Fig. 6. Note that for 2-soliton solution we have $\boldsymbol{W}^n \neq \boldsymbol{0}$ in general in which case the Lagrange multiplier is required to ensure $\int_{\mathbb{S}^1} \boldsymbol{V}^n \cdot \boldsymbol{W}^n = 0$ for all n and that the results of Theorem 4.7 hold.

5.5. Test 3 – dynamics of 2 and 3-soliton solutions

Subtest 1. We take $d = 2$ and

$$\boldsymbol{u}_0 = \frac{F_{\mu,\nu}}{G}\boldsymbol{E}_1 + \frac{F_{\nu,\mu}}{G}\boldsymbol{E}_2, \tag{5.6}$$

with $F_{\mu,\nu}$ given in (2.26) G given in (2.27). The parameters are $\boldsymbol{E_1} = (\frac{9}{10}, \frac{\sqrt{19}}{10})^\intercal$, $\boldsymbol{E_2} = (\frac{1}{10}, \frac{3\sqrt{11}}{10})^\intercal$, $\mu = \sqrt{2}$, $\nu = \sqrt{3}$, $c_\nu = 10$, $c_\mu = 13$. Fig. 8 shows some plots of the dynamics of the numerical approximation.

Subtest 2. We take $d = 2$ and

$$\boldsymbol{u}_0 = \frac{F_{\mu,\nu}}{G}\boldsymbol{E}_1 + \frac{F_{\nu,\mu}}{G}\boldsymbol{E}_2, \tag{5.7}$$

with $F_{\mu,\nu}$ given in (2.26) G given in (2.27). The parameters are $\boldsymbol{E_1} = (1,0)^\intercal$, $\boldsymbol{E_2} = (0,1)^\intercal$, $\mu = -\sqrt{2}$, $\nu = \sqrt{3}$, $c_\mu = 9$, $c_\nu = 13$. Fig. 9 shows some plots of the dynamics of the numerical approximation. We also examine the difference in the amplitude and phase between the numerical and exact solitons in each vector component before and after the soliton interaction in Table 1. The amplitude and phase errors are calculated as described in the one soliton case.

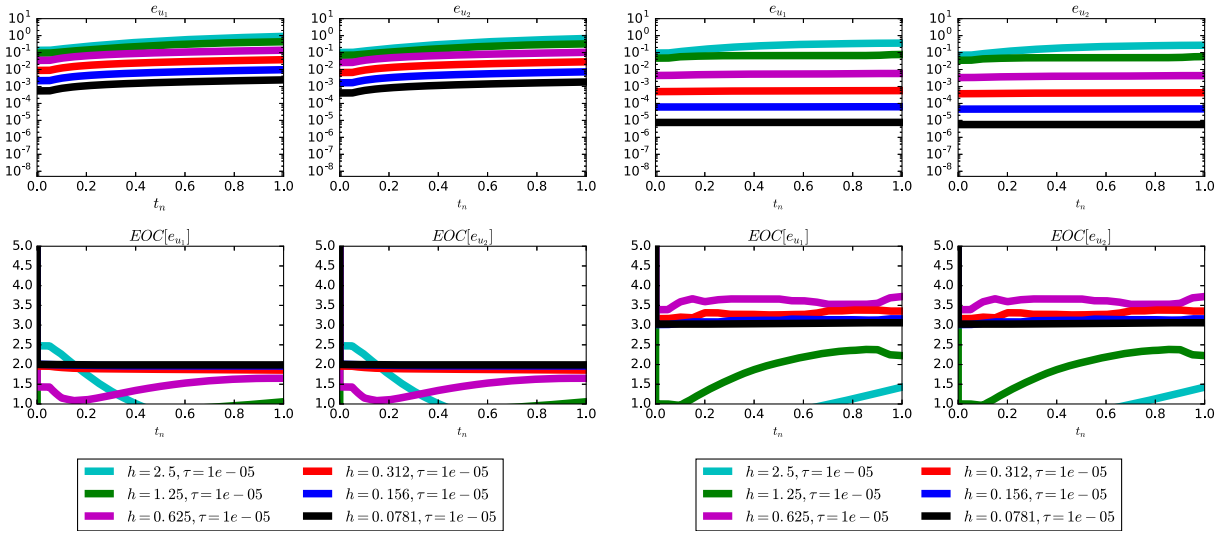

(a) Here $q = 1$ and we fix $\tau = 0.00001$. This is sufficiently small that the spatial discretisation error dominates.

(b) Here $q = 2$ and we fix $\tau = 0.00001$. This is sufficiently small that the spatial discretisation error dominates.

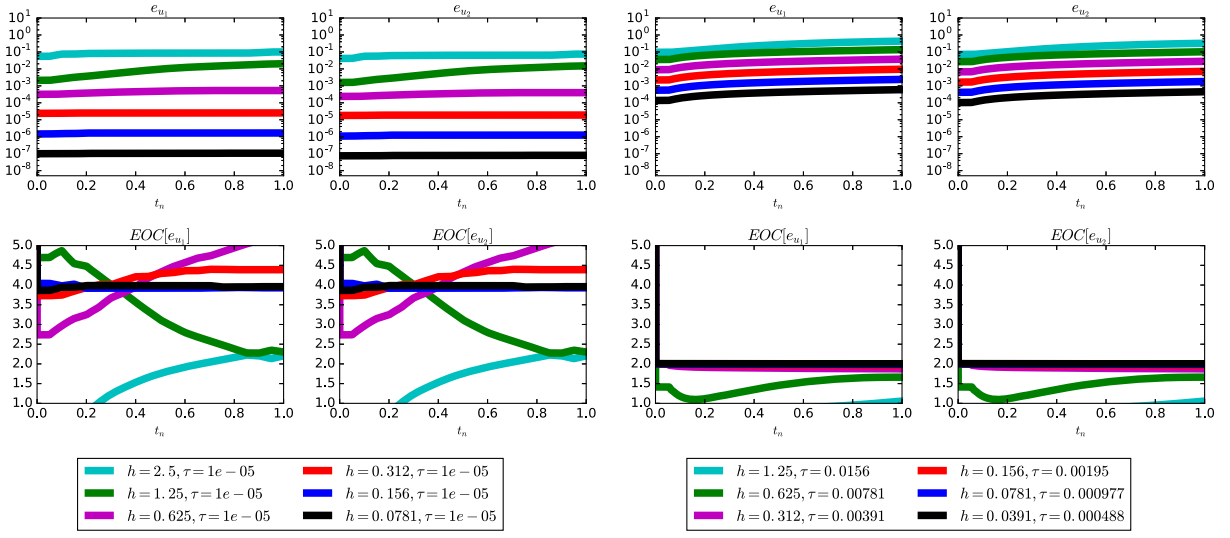

(c) Here $q = 3$ and we fix $\tau = 0.00001$. This is sufficiently small that the spatial discretisation error dominates.

(d) Here $q = 2$ and on every refinement level we choose a coupling $\tau = Ch$. Note that the time discretisation error here dominates.

Fig. 2. Here we examine the conservative discretisation scheme with various polynomial degrees, q, approximating the exact solution (2.24) with initial conditions given by (5.2). We show the errors measured in the $\mathrm{L}^\infty(0, t_n; \mathrm{L}^2(\mathbb{S}^1))$ norm for each component of the system and the EOC for test runs that benchmark both the spatial and temporal discretisation and show that the scheme is of optimal order. We use $e_{u_i} := \|u_i - U_i\|_{\mathrm{L}^\infty(0,t_n;\mathrm{L}^2(\mathbb{S}^1))}$ for $i = 1, 2$, the components of the solution $\boldsymbol{u} = (u_1, u_2)^\intercal$ and numerical approximation $\boldsymbol{U} = (U_1, U_2)^\intercal$.

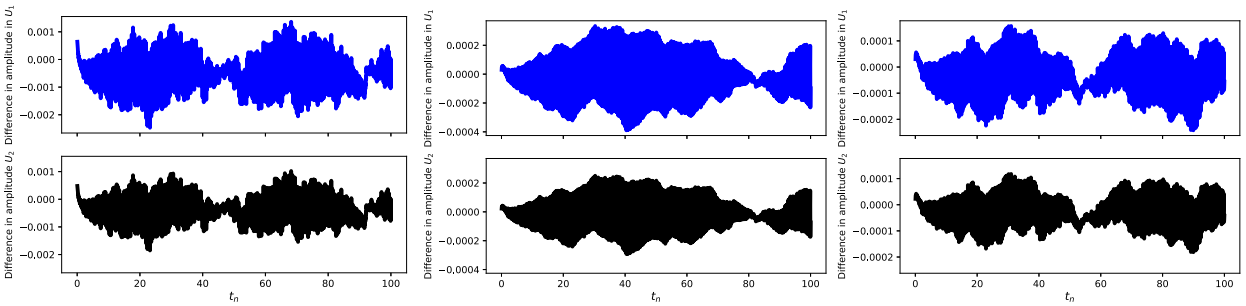

(a) Here $q = 1$. (b) Here $q = 2$. (c) Here $q = 3$.

Fig. 3. We examine the difference in maximal amplitude of the solutions for various polynomial degrees, q, compared to the exact solution (2.24) with initial conditions given by (5.2). When the difference in amplitude is positive the numerical approximation is larger than the exact solution, and when it is negative the numerical approximation is smaller. We plot these difference for both vector components of the soliton independently. In these simulations we take a fixed spatial discretisation parameter of $h = 0.08$ and a fixed time step of $\tau = 0.05$. We notice that the deviation in amplitude is bounded over time and decreases with polynomial degree.

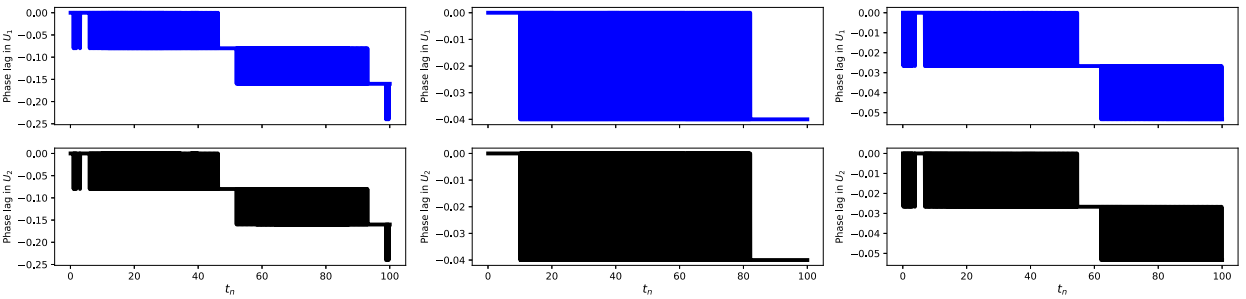

(a) Here $q = 1$. (b) Here $q = 2$. (c) Here $q = 3$.

Fig. 4. We examine the difference in speed between numerical solutions for various polynomial degrees, q, and the exact solution (2.24) with initial conditions given by (5.2). We track this difference by looking at the spatial coordinate of the maximal amplitude for the numerical and exact solutions, and take the difference. We plot these differences for both vector components of the soliton independently. In these simulations we take a fixed spatial discretisation parameter of $h = 0.08$ and a fixed time step of $\tau = 0.05$. We notice that the phase error decreases over time, i.e., the numerical solution travels slower than its exact counterpart.

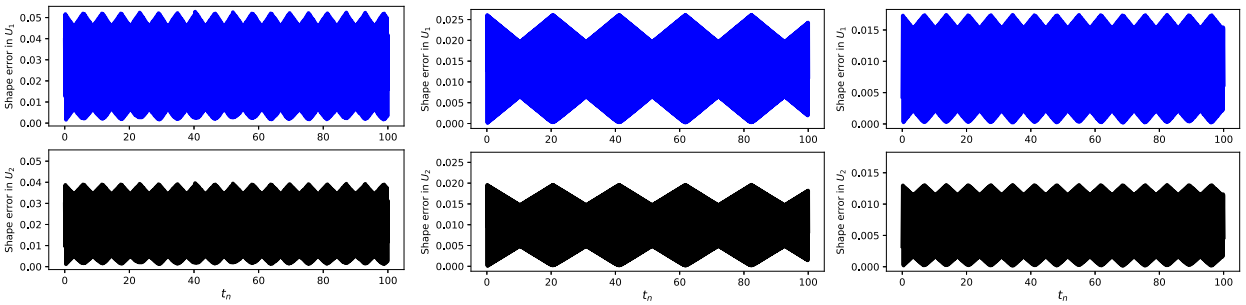

(a) Here $q = 1$. (b) Here $q = 2$. (c) Here $q = 3$.

Fig. 5. We examine the difference in the shape between numerical solutions for various polynomial degrees, q, and the exact solution (2.24) with initial conditions given by (5.2). Mathematically we can write the shape error as $\min_{y\in\mathbb{S}^1} \|u_i(x+y,t_n) - U_i(x,t_n)\|_{\mathrm{L}^2(\mathbb{S}^1)}$ for each component of the solution. In these simulations we take a fixed spatial discretisation parameter of $h = 0.08$ and a fixed time step of $\tau = 0.05$. We notice that the shape error does not propagate over long time and decreases as the polynomial degree increases.

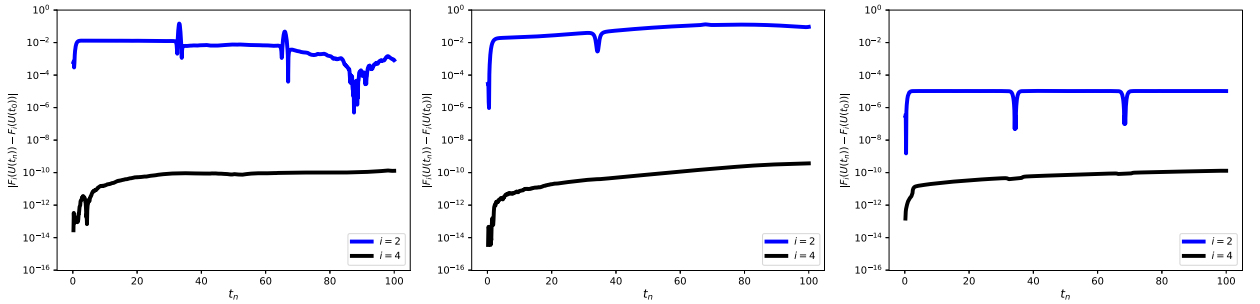

(a) Here $q = 1$. (b) Here $q = 2$. (c) Here $q = 3$.

Fig. 6. We examine the conservative discretisation scheme with various polynomial degrees, q, approximating the exact solution (2.25) with initial conditions given by (5.5). We show the deviation in the two invariants F_i, $i = 2, 4$, corresponding to momentum and energy respectively. In each test we take a fixed spatial discretisation parameter of $h = 0.25$ and fixed time step of $\tau = 0.001$. Notice that in each case the deviation in energy is smaller than the solver tolerance of 10^{-12} and the deviation in momentum is bounded. The simulations are simulated for long time to test conservativity with $T = 100$ in each case.

Table 1
The phase and amplitude errors committed by the conservative discretisation scheme approximating the smooth solution (5.7). We display the minimal and maximal errors both before and after the soliton interactions for various coupled temporal and spatial discretisations and various polynomial degrees. We notice, as in the one soliton case, our numerical solitons travel slower than their exact counterparts both before and after soliton interactions, with the phase error generally increasing after the soliton interactions. Note that when the phase error is measured to be zero this *does not* mean that the phase of the numerical scheme is exact, only that the phase error is smaller than the distance between the degrees of freedom, $\frac{h}{q}$, of our numerical approximation. The error in amplitude also increases after the soliton interaction, but remains reasonably small and decreases with the polynomial degree.

Phase and amplitude errors for the first vector component of the solution.

τ	h	Degree	Phase error for $t \in [0, 2.0]$		Phase error for $t \in [6.0, 8.0]$		Amplitude error for $t \in [0, 2.0]$		Amplitude error for $t \in [6.0, 8.0]$	
			min	max	min	max	min	max	min	max
		1	−3.2e−01	0.0e+00	−1.3e+00	−6.4e−01	−2.5e−01	3.2e−03	−2.6e−01	2.1e−02
2.0e−02	3.2e−01	2	−1.6e−01	0.0e+00	−1.6e−01	0.0e+00	−2.0e−02	8.8e−03	−3.9e−02	2.3e−02
		3	−1.1e−01	0.0e+00	−1.1e−01	0.0e+00	−6.2e−03	4.3e−03	−1.4e−02	1.2e−02
		1	−1.6e−01	0.0e+00	−4.8e−01	−1.6e−01	−7.0e−02	−3.8e−03	−7.6e−02	−6.1e−03
1.0e−02	1.6e−01	2	0.0e+00	0.0e+00	−8.0e−02	0.0e+00	−2.1e−03	1.2e−03	−4.4e−03	2.8e−03
		3	−5.3e−02	0.0e+00	−5.3e−02	0.0e+00	−7.9e−04	7.7e−04	−2.3e−03	2.2e−03
		1	−8.0e−02	0.0e+00	−8.0e−02	0.0e+00	−1.6e−02	−5.7e−04	−1.8e−02	−4.8e−03
5.0e−03	8.0e−02	2	−4.0e−02	0.0e+00	0.0e+00	0.0e+00	−2.2e−04	1.1e−04	−5.3e−04	3.7e−04
		3	−2.7e−02	0.0e+00	−2.7e−02	0.0e+00	−1.2e−04	7.7e−05	−3.5e−04	2.7e−04
		1	−4.0e−02	0.0e+00	−4.0e−02	0.0e+00	−3.5e−03	−5.9e−05	−4.9e−03	4.0e−05
2.5e−03	4.0e−02	2	−2.0e−02	0.0e+00	0.0e+00	0.0e+00	−2.6e−05	1.4e−05	−7.6e−05	3.6e−05
		3	−1.3e−02	0.0e+00	−1.3e−02	0.0e+00	−1.9e−05	1.1e−05	−5.6e−05	3.5e−05

Phase and amplitude errors for the second vector component of the solution.

τ	h	Degree	Phase error for $t \in [0, 2.0]$		Phase error for $t \in [6.0, 8.0]$		Amplitude error for $t \in [0, 2.0]$		Amplitude error for $t \in [6.0, 8.0]$	
			min	max	min	max	min	max	min	max
		1	−3.2e−01	0.0e+00	−9.6e−01	−3.2e−01	−1.4e−01	−1.2e−02	−1.0e−01	−9.3e−03
2.0e−02	3.2e−01	2	0.0e+00	0.0e+00	0.0e+00	0.0e+00	−5.0e−03	1.2e−03	−7.5e−03	3.9e−03
		3	0.0e+00	0.0e+00	−1.1e−01	0.0e+00	−8.2e−04	7.2e−04	−2.9e−03	2.8e−03
		1	−1.6e−01	0.0e+00	−3.2e−01	0.0e+00	−3.2e−02	−1.1e−03	−2.8e−02	−4.4e−03
1.0e−02	1.6e−01	2	−8.0e−02	0.0e+00	0.0e+00	0.0e+00	−4.0e−04	1.9e−04	−3.3e−04	2.9e−04
		3	0.0e+00	0.0e+00	0.0e+00	0.0e+00	−1.2e−04	7.0e−05	−3.5e−04	4.9e−04
		1	−8.0e−02	0.0e+00	−8.0e−02	0.0e+00	−7.0e−03	−1.9e−04	−9.1e−03	1.6e−03
5.0e−03	8.0e−02	2	0.0e+00	0.0e+00	0.0e+00	0.0e+00	−3.9e−05	1.8e−05	−1.4e−05	9.7e−05
		3	0.0e+00	0.0e+00	0.0e+00	0.0e+00	−1.9e−05	1.0e−05	−4.4e−05	8.0e−05
		1	−4.0e−02	0.0e+00	−4.0e−02	0.0e+00	−1.5e−03	−2.0e−05	−2.1e−03	7.0e−05
2.5e−03	4.0e−02	2	0.0e+00	0.0e+00	0.0e+00	0.0e+00	−7.6e−06	7.7e−06	−5.7e−07	2.7e−05
		3	0.0e+00	0.0e+00	0.0e+00	0.0e+00	−3.4e−06	2.1e−06	−5.6e−06	1.5e−05

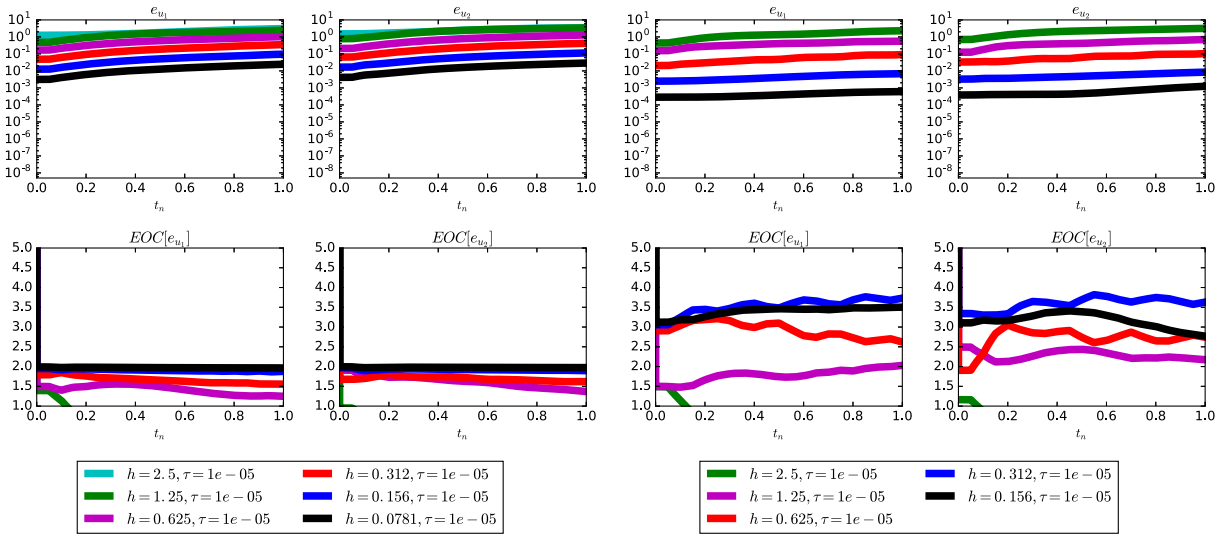

(a) Here $q = 1$ and we fix $\tau = 0.00001$. This is sufficiently small that the spatial discretisation error dominates.

(b) Here $q = 2$ and we fix $\tau = 0.00001$. This is sufficiently small that the spatial discretisation error dominates.

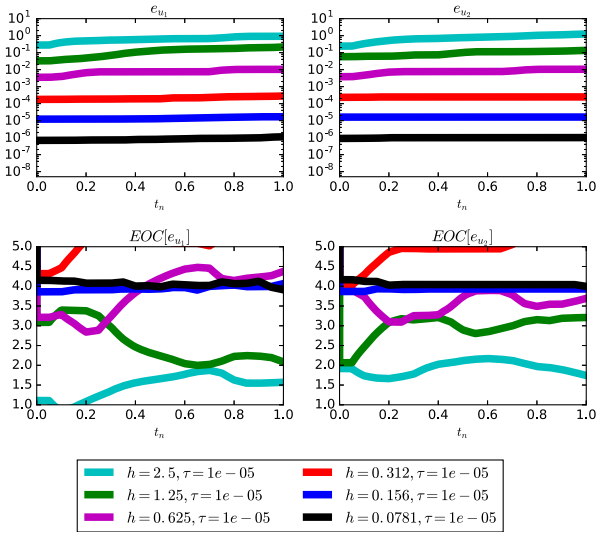

(c) Here $q = 3$ and we fix $\tau = 0.00001$. This is sufficiently small that the spatial discretisation error dominates.

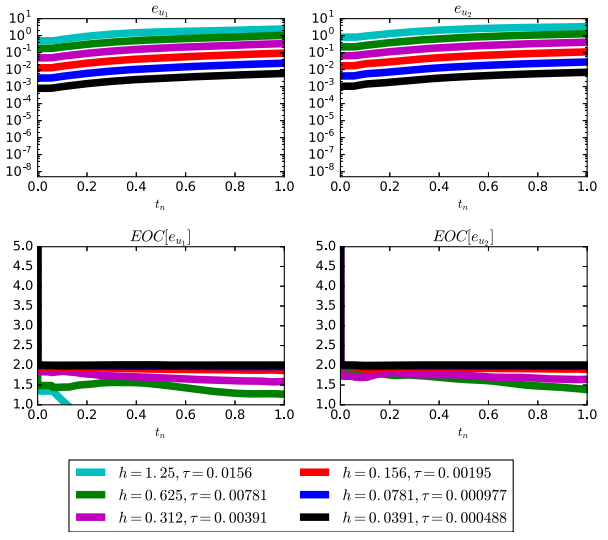

(d) Here $q = 2$ and on every refinement level we choose a coupling $\tau = Ch$. Note that the time discretisation error here dominates.

Fig. 7. We examine the conservative discretisation scheme with various polynomial degrees, q, approximating the exact solution (2.25) with initial conditions given by (5.5). We show the errors measured in the $\mathrm{L}^\infty(0, t_n; \mathrm{L}^2(\mathbb{S}^1))$ norm for each component of the system and the EOC for test runs that benchmark both the spatial and temporal discretisation and show that the scheme is of the correct order. We use $e_{u_i} := \|u_i - U_i\|_{\mathrm{L}^\infty(0,t_n;\mathrm{L}^2(\mathbb{S}^1))}$ for $i = 1, 2$, the components of the solution $\boldsymbol{u} = (u_1, u_2)^\intercal$.

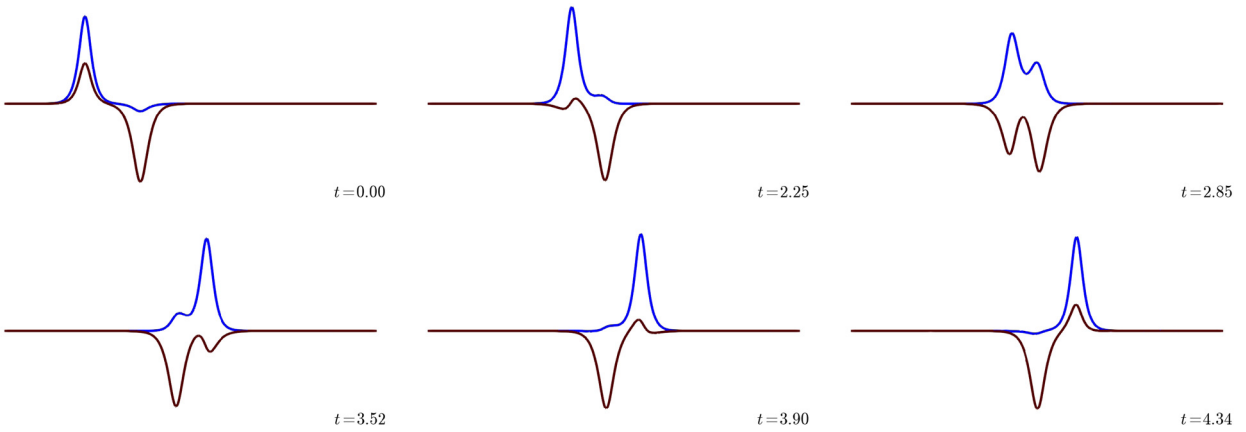

Fig. 8. The dynamics of the approximation generated by the conservative discretisation scheme with polynomial degree $q = 1$ approximating a smooth solution with initial conditions given by (5.6).

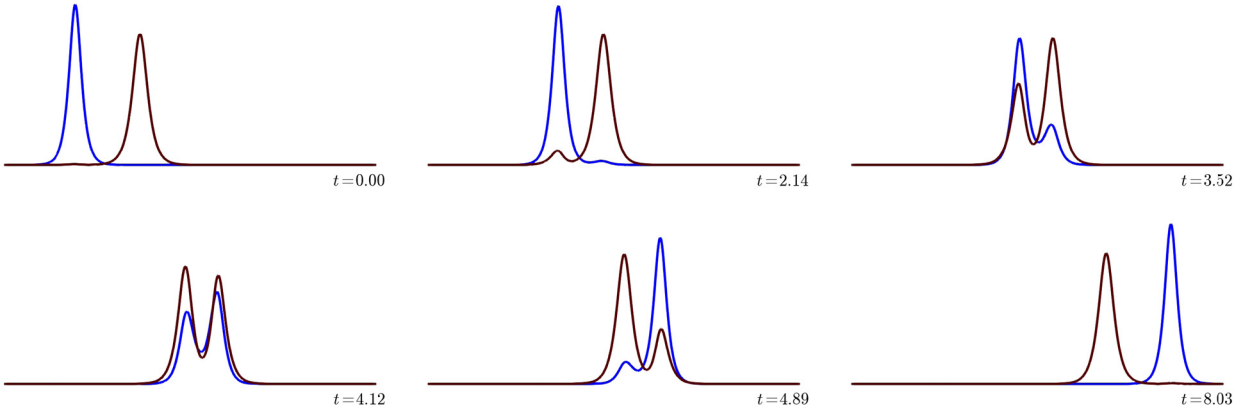

Fig. 9. The dynamics of the approximation generated by the conservative discretisation scheme with polynomial degree $q = 1$ approximating a smooth solution with initial conditions given by (5.7).

Subtest 3. In addition to the 2-soliton interactions we also take the opportunity to examine the dynamics of a 3-soliton interaction. We take $d = 2$ and

$$\boldsymbol{u}_0 = \sum_{i=1}^{3} \frac{2\mu_i}{\cosh\left(\mu_i\left(x - c_{\mu_i}\right)\right)} \boldsymbol{E_i} \tag{5.8}$$

with $\boldsymbol{E}_1 = \boldsymbol{E}_3 = (1,0)^\intercal$, $\boldsymbol{E}_2 = (0,1)^\intercal$, $\mu_1 = \frac{19}{10}, \mu_2 = -\frac{40}{25}, \mu_3 = \frac{13}{10}$ and $c_{\mu_1} = 4, c_{\mu_2} = 12, c_{\mu_3} = 21$. Fig. 10 shows the dynamics of the numerical approximation.

5.6. Test 4 – propagation of solitary waves from smooth initial data

We take $d = 2$ and $\boldsymbol{u}_0 = \left(u_{0,1}, u_{0,2}\right)$ with

$$\begin{aligned} u_{0,1} &= \sin\left(\frac{\pi}{20}x\right) \\ u_{0,2} &= \cos\left(\frac{\pi}{10}x\right). \end{aligned} \tag{5.9}$$

The solution here is smooth and solitary waves begin to form quickly into the simulation (see Fig. 12). Plots of the solutions are given in Fig. 13 as well as conservativity plots in Figs. 11, 12.

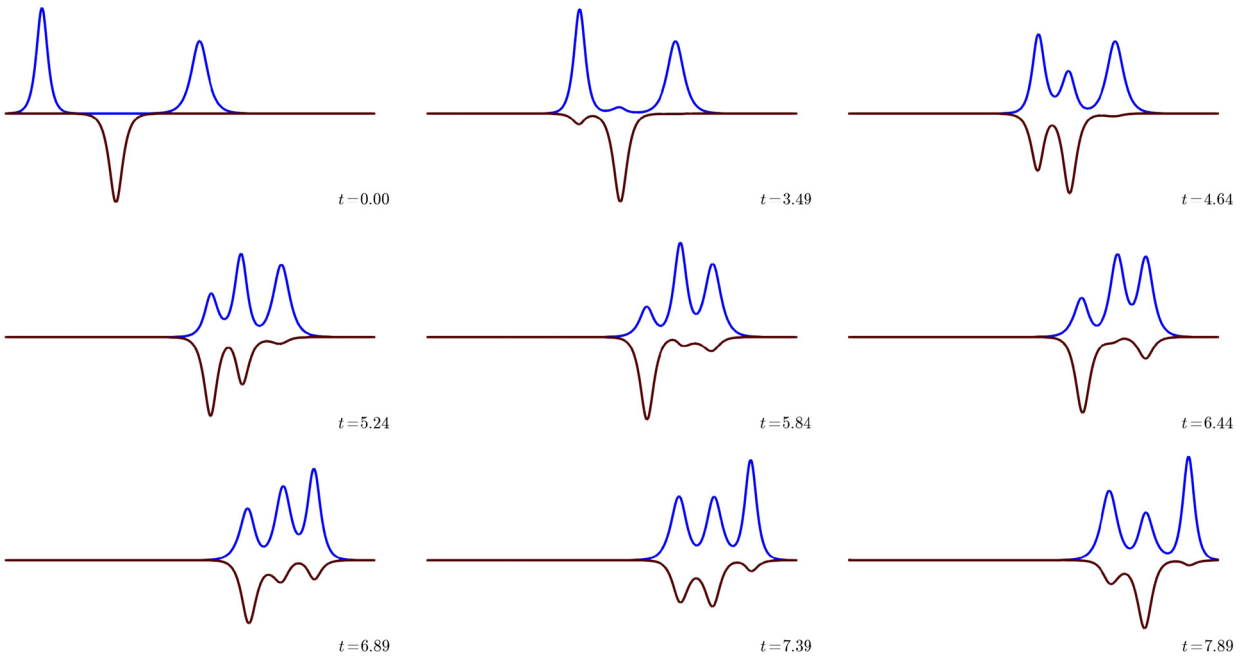

Fig. 10. The dynamics of the approximation generated by the conservative discretisation scheme with polynomial degree $q = 1$ approximating a smooth solution with initial conditions given by (5.8).

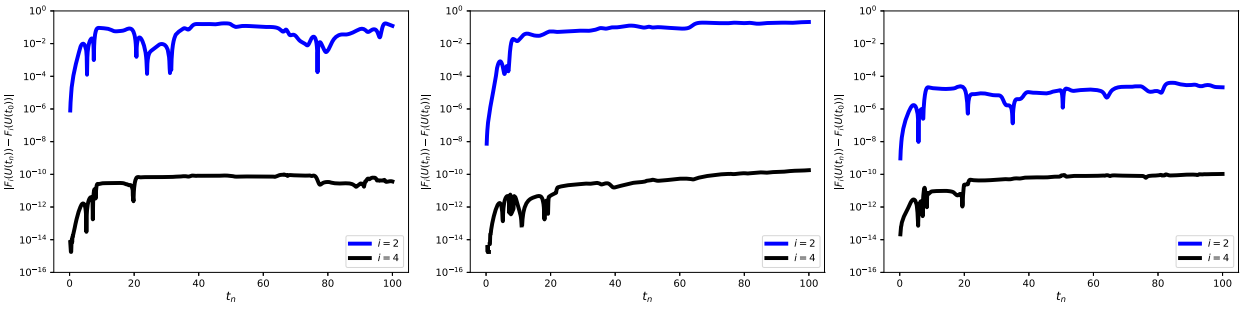

(a) $q = 1$ (b) $q = 2$ (c) $q = 3$

Fig. 11. The conservative discretisation scheme with various polynomial degrees, q, approximating the solution to (2.2) with initial conditions given by (5.9). We show the deviation in the two invariants F_i, $i = 2, 4$, corresponding to momentum and energy respectively. In each test we take a fixed spatial discretisation parameter of $h = 0.25$ and fixed time step of $\tau = 0.001$. Notice that in each case the deviation in energy is smaller than the solver tolerance of 10^{-12} and the deviation in momentum is bounded. The simulations are simulated for long time to test conservativity with $T = 100$ in each case.

5.7. Test 5 – solution with discontinuous initial data

We take $d = 2$ and $\boldsymbol{u}_0 = \left(u_{0,1}, u_{0,2}\right)$ with

$$u_{0,1} = \begin{cases} 1 \text{ for } x \in [10, 20] \\ 0 \text{ otherwise.} \end{cases}$$
$$u_{0,2} = \begin{cases} 0 \text{ for } x \in [20, 30] \\ 1 \text{ otherwise.} \end{cases} \tag{5.10}$$

The solution here is discontinuous in both components. This is a particularly tough scenario to simulate as there is no guarantee of classical solutions. We align the mesh to the discontinuities so that the discrete energy at the initial condition makes sense. Plots of the solutions are given in Fig. 15 as well as conservativity plots in Fig. 14. The phenomena demon-

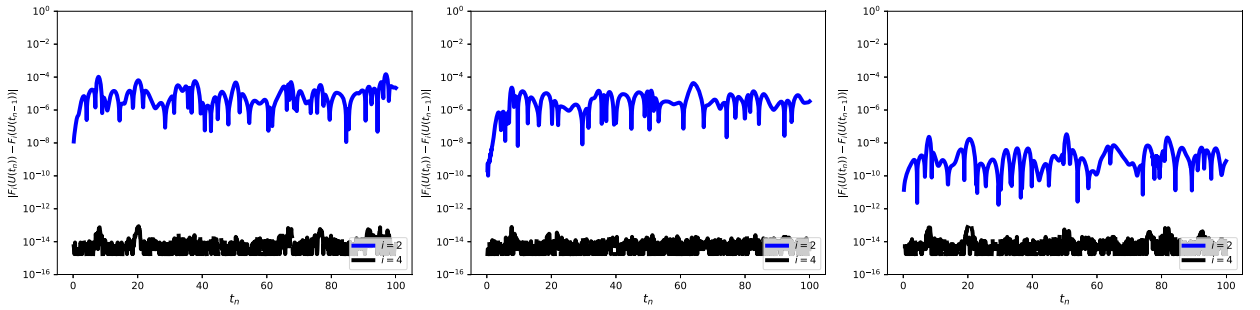

(a) $q = 1$ (b) $q = 2$ (c) $q = 3$

Fig. 12. The conservative scheme with various polynomial degrees, q, approximating the solution to (2.2) with initial conditions given by (5.9). We now show the deviation in the two invariants F_i, $i = 2, 4$, *locally*, that is, for each n, we measure $\left|F_4(U^n) - F_4(U^{n-1})\right|$. In each test we take a fixed spatial discretisation parameter of $h = 0.25$ and fixed time step of $\tau = 0.001$. Notice that in each case the deviation in energy is smaller than the solver tolerance of 10^{-12} and the deviation in momentum is bounded. The simulations run over long time to test conservativity with $T = 100$ in each case. This result should be compared to the study of the global deviation $\left|F_4(U^n) - F_4(U^0)\right|$ given in Fig. 11 which accumulates in time through propagation of precision errors over time.

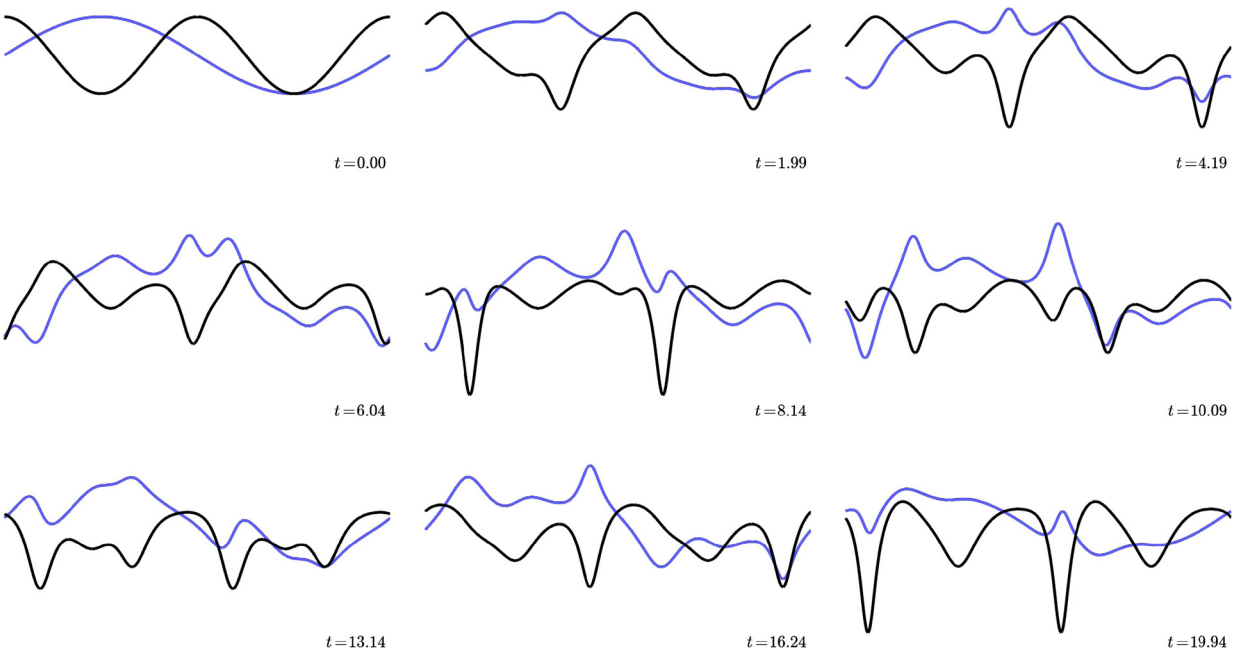

Fig. 13. Here we show the dynamics of the approximation generated by the conservative discretisation scheme with polynomial degree $q = 1$ approximating the solution to (2.2) with initial conditions given by (5.9). Notice that initially, dispersive waves emanate from the discontinuity.

strated in this experiment are related to the observations in [19] where, for the scalar KdV equation, arguments based on Whitham's modulation theory are presented.

6. Conclusions

In this work we have constructed a Galerkin approximation for the vmKdV equation that is consistent with the underlying algebraic structure of the PDE. We have proven that both the semi-discretisations as well as the fully discrete problems are conservative and numerically shown that this is true in practice. In addition, we have given numerical evidence to suggest that the method is of optimal order, that is, $\|\boldsymbol{u} - \boldsymbol{U}\|_{\mathrm{L}^\infty((0,T);\mathrm{L}^2(\mathbb{S}^1))} = \mathrm{O}(\tau^2 + h^{q+1})$. We expect methods designed in this fashion, which is quite generic, to be successful in the simulation of geophysical fluid flows.

Extensions to this work will be carried out by exploring applications to further Hamiltonian systems, a thorough error analysis, and exploiting the possibility of constructing schemes with multiple conserved quantities, see [24].

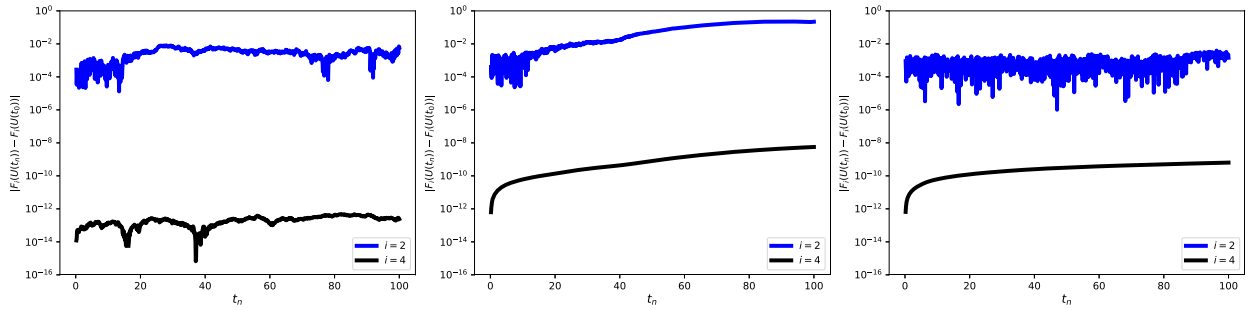

(a) $q = 1$ (b) $q = 2$ (c) $q = 3$

Fig. 14. Here we examine the conservative discretisation scheme with various polynomial degrees, q, approximating the solution to (2.2) with initial conditions given by (5.10). We show the deviation in the two invariants F_i, $i = 2, 4$, corresponding to momentum and energy respectively. In each test we take a fixed spatial discretisation parameter of $h = 0.25$ and fixed time step of $\tau = 0.001$. Notice that in each case the deviation in energy is smaller than the solver tolerance of 10^{-12} and the deviation in momentum is bounded. The simulations are simulated for long time to test conservativity with $T = 100$ in each case.

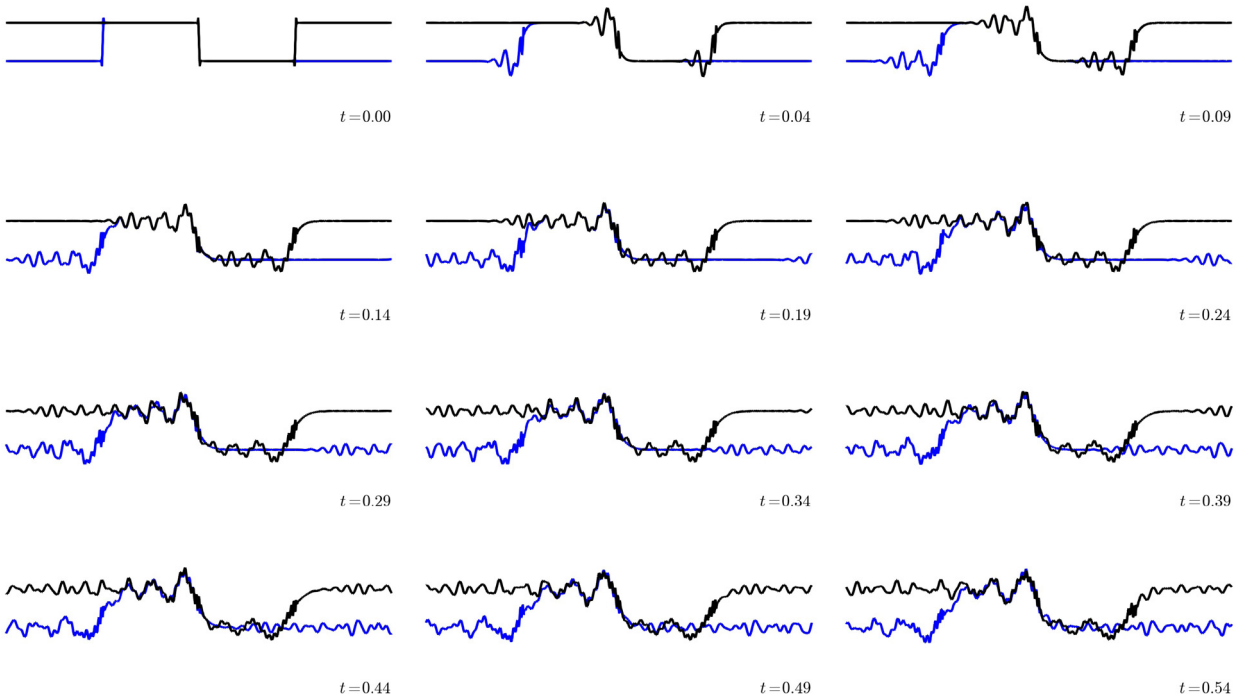

Fig. 15. Here we show the dynamics of the approximation generated by the conservative discretisation scheme with polynomial degree $q = 1$ approximating the solution to (2.2) with initial conditions given by (5.10). Notice that initially, dispersive waves emanate from the discontinuity.

References

[1] M.J. Ablowitz, P.A. Clarkson, Solitons, Nonlinear Evolution Equations and Inverse Scattering, vol. 149, Cambridge University Press, 1991.
[2] S.C. Anco, Hamiltonian flows of curves in g/so (n) and vector soliton equations of mKdV and sine-Gordon type, SIGMA 2 (2006).
[3] Stephen C. Anco, Nestor Tchegoum Ngatat, Mark Willoughby, Interaction properties of complex modified Korteweg–de Vries (mKdV) solitons, Physica D 240 (17) (2011) 1378–1394.
[4] D. Bai, L. Zhang, The finite element method for the coupled Schrödinger–KdV equations, Phys. Lett. A 373 (26) (2009) 2237–2244.
[5] Satish Balay, William D. Gropp, Lois Curfman McInnes, Barry F. Smith, Efficient management of parallelism in object oriented numerical software libraries, in: E. Arge, A.M. Bruaset, H.P. Langtangen (Eds.), Modern Software Tools in Scientific Computing, Birkhäuser Press, 1997, pp. 163–202.
[6] Satish Balay, Shrirang Abhyankar, Mark F. Adams, Jed Brown, Peter Brune, Kris Buschelman, Lisandro Dalcin, Victor Eijkhout, William D. Gropp, Dinesh Kaushik, Matthew G. Knepley, Dave A. May, Lois Curfman McInnes, Richard Tran Mills, Todd Munson, Karl Rupp, Patrick Sanan, Barry F. Smith, Stefano Zampini, Hong Zhang, Hong Zhang, PETSc Users Manual, Technical Report ANL-95/11 – Revision 3.9, Argonne National Laboratory, 2018.
[7] S. Blanes, F. Casas, A Concise Introduction to Geometric Numerical Integration, CRC Press, 2016.
[8] O. Bokhove, P. Lynch, Air parcels and air particles: Hamiltonian dynamics, Nieuw Arch. Wiskd. (5) 8 (2) (2007) 100–106.
[9] J.L. Bona, V.A. Dougalis, O.A. Karakashian, W.R. McKinney, Conservative, high-order numerical schemes for the generalized Korteweg–de Vries equation, Philos. Trans. R. Soc. Lond. Ser. A 351 (1695) (1995) 107–164.
[10] J.L. Bona, V.A. Dougalis, D.E. Mitsotakis, Numerical solution of KdV–KdV systems of Boussinesq equations: I. The numerical scheme and generalized solitary waves, Math. Comput. Simul. 74 (2) (2007) 214–228.

[11] J.L. Bona, H. Chen, O. Karakashian, Y. Xing, Conservative, discontinuous Galerkin-methods for the generalized Korteweg–de Vries equation, Math. Comput. 82 (283) (2013) 1401–1432.
[12] T.J. Bridges, S. Reich, Multi-symplectic integrators: numerical schemes for Hamiltonian PDEs that conserve symplecticity, Phys. Lett. A 284 (4–5) (2001) 184–193.
[13] E. Celledoni, V. Grimm, R.I. Mclachlan, D.I. Mclaren, D. O'Neale, B. Owren, G.R.W. Quispel, Preserving energy resp. dissipation in numerical pdes using the "average vector field" method, J. Comput. Phys. 231 (20) (August 2012) 6770–6789.
[14] D. Cohen, B. Owren, X. Raynaud, Multi-symplectic integration of the Camassa–Holm equation, J. Comput. Phys. 227 (11) (2008) 5492–5512.
[15] D. Cohen, T. Matsuo, X. Raynaud, A multi-symplectic numerical integrator for the two-component Camassa–Holm equation, J. Nonlinear Math. Phys. 21 (3) (2014) 442–453.
[16] L.D. Faddeev, L. Takhtajan, Hamiltonian Methods in the Theory of Solitons, Springer Science & Business Media, 2007.
[17] Jan Giesselmann, Tristan Pryer, Energy consistent discontinuous Galerkin methods for a quasi-incompressible diffuse two phase flow model, ESAIM: M2AN 49 (1) (2015) 275–301.
[18] Jan Giesselmann, Charalambos Makridakis, Tristan Pryer, Energy consistent discontinuous Galerkin methods for the Navier–Stokes–Korteweg system, Math. Comput. 83 (289) (2014) 2071–2099.
[19] Tamara Grava, Whitham modulation equations and application to small dispersion asymptotics and long time asymptotics of nonlinear dispersive equations, in: Rogue and Shock Waves in Nonlinear Dispersive Media, Springer, 2016, pp. 309–335.
[20] E. Hairer, C. Lubich, G. Wanner, Structure-preserving algorithms for ordinary differential equations, in: Geometric Numerical Integration, second edition, in: Springer Ser. Comput. Math., vol. 31, Springer-Verlag, Berlin, 2006.
[21] Ryogo Hirota, Exact envelope-soliton solutions of a nonlinear wave equation, J. Math. Phys. 14 (7) (1973) 805–809.
[22] R. Hirota, The Direct Method in Soliton Theory, vol. 155, Cambridge University Press, 2004.
[23] J. Jackaman, A conservative Galerkin method for the vectorial modified Korteweg de Vries equation, https://doi.org/10.5281/zenodo.600668, 2017.
[24] J. Jackaman, T. Pryer, Conservative Galerkin methods for dispersive Hamiltonian problems, ArXiV preprint, https://arxiv.org/abs/1811.09999, 2018.
[25] O. Karakashian, Ch. Makridakis, A posteriori error estimates for discontinuous Galerkin methods for the generalized Korteweg–de Vries equation, Math. Comput. 84 (293) (2015) 1145–1167.
[26] Emine Kesici, Beatrice Pelloni, Tristan Pryer, David Smith, A numerical implementation of the unified Fokas transform for evolution problems on a finite interval, Eur. J. Appl. Math. 29 (3) (2018) 543–567.
[27] P.D. Lax, Almost periodic solutions of the KdV equation, SIAM Rev. 18 (3) (1976) 351–375.
[28] B. Leimkuhler, S. Reich, Simulating Hamiltonian Dynamics, Cambridge Monogr. Appl. Comput. Math., vol. 14, Cambridge University Press, Cambridge, 2004.
[29] Franco Magri, A simple model of the integrable hamiltonian equation, J. Math. Phys. 19 (5) (1978) 1156–1162.
[30] G. Mari Beffa, Jan A. Sanders, Jing Ping Wang, Integrable systems in three-dimensional riemannian geometry, J. Nonlinear Sci. 12 (2) (2002) 143–167.
[31] P. Müller, C. Garrett, A. Osborne, Rogue waves, Oceanography 18 (3) (2005) 66–75.
[32] S. Novikov, S.V. Manakov, L.P. Pitaevskii, V.E. Zakharov, Theory of Solitons: the Inverse Scattering Method, Springer Science & Business Media, 1984.
[33] P.J. Olver, Applications of Lie Groups to Differential Equations, second edition, Grad. Texts Math., vol. 107, Springer-Verlag, New York, 1993.
[34] Florian Rathgeber, David A. Ham, Lawrence Mitchell, Michael Lange, Fabio Luporini, Andrew T.T. McRae, Gheorghe-Teodor Bercea, Graham R. Markall, Paul H.J. Kelly, Firedrake: automating the finite element method by composing abstractions, ACM Trans. Math. Softw. 43 (3) (2016) 24.
[35] S. Reich, Finite volume methods for multi-symplectic PDEs, BIT Numer. Math. 40 (3) (2000) 559–582.
[36] C. Rogers, W.K. Schief, Bäcklund and Darboux Transformations: Geometry and Modern Applications in Soliton Theory, vol. 30, Cambridge University Press, 2002.
[37] I. Roulstone, J. Norbury, A Hamiltonian structure with contact geometry for the semi-geostrophic equations, J. Fluid Mech. 272 (1994) 211–233.
[38] M.A. Salle, V.B. Matveev, Darboux Transformations and Solitons, 1991.
[39] Jan A. Sanders, Jing Ping Wang, Integrable systems in n-dimensional riemannian geometry, Mosc. Math. J. 3 (4) (2003) 1369–1393.
[40] T.G. Shepherd, Symmetries, conservation laws, and Hamiltonian structure in geophysical fluid dynamics, Adv. Geophys. 32 (1990) 287–338.
[41] R. Winther, A conservative finite element method for the Korteweg–de Vries equation, Math. Comput. 34 (149) (1980) 23–43.
[42] Y. Xu, C.W. Shu, Error estimates of the semi-discrete local discontinuous Galerkin method for nonlinear convection–diffusion and KdV equations, Comput. Methods Appl. Mech. Eng. 196 (37–40) (2007) 3805–3822.
[43] J. Yan, C.W. Shu, A local discontinuous Galerkin method for KdV type equations, SIAM J. Numer. Anal. 40 (2) (2002) 769–791 (electronic).